applied sciences

MDPI

Review

Sound Field Modeling Method and Key Imaging Technology of an Ultrasonic Phased Array: A Review

Qian Xu [1,*] and Haitao Wang [1,2,*]

[1] College of Automation Engineering, Nanjing University of Aeronautics and Astronautics, Nanjing 210016, China
[2] Key Laboratory of Non-Destructive 'Testing and Monitoring' Technology for High-Speed Transport Facilities of the Ministry of Industry and Information Technology, Nanjing University of Aeronautics and Astronautics, Nanjing 210016, China
* Correspondence: xuqian_ndt@nuaa.edu.cn (Q.X.); htwang2002@126.com (H.W.)

Abstract: An ultrasonic phased array consists of multiple ultrasonic probes arranged in a certain regular order, and the delay time of the excitation signal sent to each array element is controlled electronically. The testing system model based on ultrasonic propagation theory is established to obtain a controllable and focused sound field, which has theoretical and engineering guiding significance for the calculation and analysis of ultrasonic array sound fields. Perfecting array theory and exploring array imaging methods can obtain rich acoustic information, provide more intuitive and reliable research results, and further the development of ultrasonic phased-array systems. This paper reviews the progress of research on the application of ultrasound arrays for non-destructive testing (NDT) and brings together the most relevant published work on the application of simulation methods and popular imaging techniques for ultrasonic arrays. It mainly reviews the modeling approaches, including the angular spectrum method (ASM), multi-Gaussian beam method (MGB), ray tracing method, finite element method (FEM), finite difference method (FDM), and distributed point source method (DPSM), which have been used to assess the performance and inspection modality of a given array. In addition, the array of imaging approaches, including the total focusing method (TFM), compression sensing imaging (CSI), and acoustic nonlinearity imaging (ANI), are discussed. This paper is expected to provide strong technical support in related areas such as ultrasonic array testing theory and imaging methods.

Keywords: ultrasonic phased array; modelling; total focusing method; compressed sensing; acoustic nonlinearity imaging

check for updates

Citation: Xu, Q.; Wang, H. Sound Field Modeling Method and Key Imaging Technology of an Ultrasonic Phased Array: A Review. *Appl. Sci.* **2022**, *12*, 7962. https://doi.org/10.3390/app12167962

Academic Editor: Stefano Invernizzi

Received: 2 July 2022
Accepted: 4 August 2022
Published: 9 August 2022

Publisher's Note: MDPI stays neutral with regard to jurisdictional claims in published maps and institutional affiliations.

Copyright: © 2022 by the authors. Licensee MDPI, Basel, Switzerland. This article is an open access article distributed under the terms and conditions of the Creative Commons Attribution (CC BY) license (https://creativecommons.org/licenses/by/4.0/).

1. Introduction

The maturity of array testing theory promotes its application in nondestructive testing. Ultrasonic arrays have two key advantages over standard monolithic sensors. First, a specific array can perform a range of different detections from a single location, making it more flexible than a single-cell sensor. Secondly, the array ultrasound technique allows images to be generated at each test location. This allows rapid visualization of the internal structure of the specimen. These advantages have led to the rapid adoption of arrays in the engineering industry. At present, the research on ultrasonic arrays mainly focuses on transducer development, detection, and imaging methods. A large amount of research has been published in these areas using an array of ultrasound inspection techniques.

Modeling plays a crucial role in the use of arrays for Non-Destructive Evaluation (NDE) due to the wide range of array geometries and inspection methods possible. Drinkwater et al. [1] reviewed the modeling approaches which have been adopted to assess the performance of a given array and inspection modality. Both modeling techniques are based on directly emulating the physical operation of an array. However, the development and application of several modeling methods in the non-destructive assessment of ultrasound arrays are

not well reviewed. Based on various detection and imaging modes of ultrasonic arrays, ultrasonic arrays need to study the propagation of sound field in the medium and the response of defects and explore the localization and quantification methods of defects for detection. The modeling methods include analytical approaches, numerical approaches, and semi-analytical approaches. Commonly used analytical calculation approaches include the angular spectrum method (ASM), multi-Gaussian beam method (MGB), and ray tracing method. Numerical approaches include the finite element method (FEM) and finite difference method (FDM). Semi-analytic methods include the distributed point source method (DPSM). Section 2 of this paper gives an overview of the basic theories of the different modeling methods and the application of these methods in ultrasonic arrays by reviewing a wide range of published research.

With the development of materials science, the requirements for inspection technology in engineering practice are constantly increasing. The needs for detection of microcracks/micro-defects, detection of complex shaped parts, detection of distal ends of large structures, detection of composite structures, detection of bonding quality, and non-destructive evaluation of the mechanical properties of materials are constantly emerging. Traditional linear ultrasound observation of time domain signals, limited by wavelength and other factors, is not sensitive to micro-defects, micro-cracks, and interface defects such as bonding and delamination. Non-linear ultrasound inspection technology mainly observes the non-linear acoustic response of materials and overcomes the shortcomings of traditional ultrasound by analyzing signal changes in frequency and is an effective complement to traditional linear ultrasound inspection means. Felice et al. [2] reviewed techniques for sizing defects using ultrasonic body waves, including amplitude, time, imaging, and inversion techniques, and the advantages and limitations of various techniques are compared from the perspective of principle and method, but the development and application of nonlinear effects in array ultrasound are not introduced enough.

The development and application of several detection techniques in ultrasonic arrays are reviewed in Section 3, including the total focusing method (TFM), compression sensing imaging (CSI), and acoustic nonlinearity imaging (ANI). Section 1 outlines the basic theory, correction algorithm, and acceleration algorithm of TFM as well as reviewing the industry application of the technology. Section 2 describes the theory of CSI and overviews ultrasonic array research work on the three key issues of CSI: sparse representation, observation sampling, and image reconstruction. Section 3 mainly introduces the harmonic imaging and modulation imaging methods of nonlinear ultrasonic arrays. An extensive list of references is then given; from a large amount of research work, we sort out the hotspots and difficulties of these technologies. This paper aims to provide a reference for further improving the quality of ultrasound array imaging, enriching the content and presentation of ultrasound imaging, and achieving structural health monitoring and defect life assessment research.

2. Modelling Method

The establishment of an ultrasonic array mathematical model not only helps us to understand the propagation process of acoustic waves and the interaction between acoustic waves and defects, but also guides us to design excellent ultrasonic sensors, obtain the best detection effect, and extract accurate and rich acoustic characteristic information [3].

2.1. Angular Spectrum Method

ASM was introduced from the field of optics to the field of acoustics in the 1970s [4]. It is a standard method to extrapolate the ultrasonic field from the point measurement data set of the pressure field in a single plane. First, the propagation and attenuation of numerous plane waves emitted by the probe in the medium are calculated. Then, the propagation of the sound field is simulated by dividing all the superimposed plane waves by a certain weight function. Similar to the Rayleigh integral, ASM is the spatial frequency-domain representation of Huygens' Principle [5]. It has been widely used in sensor modeling and analysis, and more and more attention is paid to it. ASM can also be

used to deal with complex situations, such as the distribution of sound fields in anisotropic media, and the transmission and reflection of sound beams across curved interfaces. The principle of the traditional angular spectrum method is shown in Figure 1.

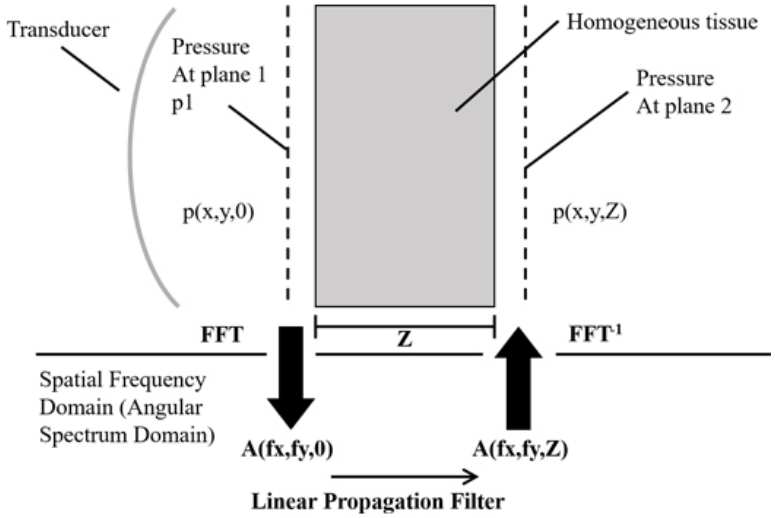


Figure 1. Traditional angular spectrum method.

A measurement technique for analyzing the velocity distribution on ultrasonic surfaces was proposed in 1989, which was based on the angular spectrum method of wave [6]. In 2008, Belgroune et al. [7] developed a model for studying transient ultrasonic waves radiated by a transducer in a liquid and transmitted through a planar interface to a solid. This extends the transient situation of the ASM developed for the monochrome situation. In 2012, the ASM was extended to non-uniform tissues. The hybrid angular spectrum (HAS) method was proposed by Vyas et al. [8,9]. The approach proposes an inhomogeneous medium modeled using voxels, and its principle is shown in Figure 2. Each voxel has a unique sound velocity, absorption coefficient, and density. To find the pressure diagram at a distance from the input pressure diagram Z, the calculation of each layer alternates between the spatial domain and the frequency domain. In the spatial domain, the result of multiplying the pressure field at the entrance of the layer by the transfer function is subjected to a Fourier transform and then multiplied by the linear propagation term representing the average phase shift of the interlayer distance. The initial pressure field is transformed by FFT into a wave spectrum $A_1^*(a, \beta)$ into plane 1, which is then transformed by FFT after multiplying by a linear propagation term representing the distance between the layers into a spatial domain pressure field, where it becomes the pressure field at the entrance to plane2. We can model complex and irregular inhomogeneous tissue geometries and quickly and accurately calculate the complex pressure distribution in a non-uniform three-dimensional model through controlling the size and number of voxels. Then, in 2017, Ilyina et al. [10] calculated the pressure field of the cylindrical bending transducer array and compared the numerical results with those obtained through Field II. Meanwhile, they verified the accuracy of the method proposed by Vyas et al. When using the ASM to calculate the field radiated by a sound source of limited size, how to avoid or eliminate the aliasing phenomenon in the frequency domain and the distortion caused by the phase shift will be the focus of research.

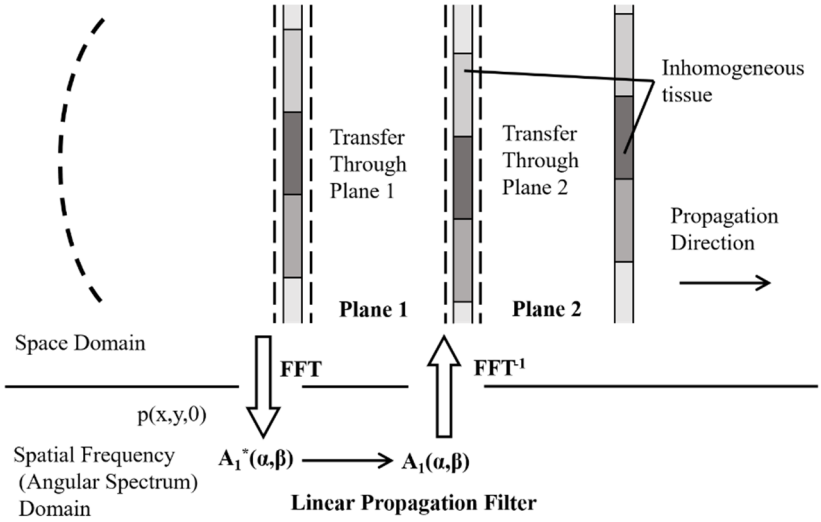


Figure 2. Hybrid angular spectrum method.

2.2. Multi-Gaussian Beam Method

In general, many spherical or plane waves need to be superimposed in the calculation of the probe emission acoustic field. However, The sound field of plane probe and focus probe can be simulated by using a small number of Gaussian beam superposition. The boundary condition of multiple single Gaussian acoustic beams superimposed to simulate the acoustic field of the ultrasonic probe is called Multivariate Gaussian Sound Beam (MGB). This model was derived from the Helmholtz wave equation by Wen [11] in 1988 and demonstrated that the acoustic beam radiated into the water by a circular piston probe could be accurately simulated by superimposing only ten Gaussian beams. Due to its high computational efficiency and good simulation of ultrasonic waves, MGB has been widely applied in the modeling process of ultrasonic arrays. When there is no delay and deflection, the total radiation sound field of N array elements can be obtained by the following Equation (1) [12]:

In a single medium, the Rayleigh integral of the sound field radiated by the nth rectangular source is:

$$p_n(x,\omega) = \frac{-i\omega p_1 v_0(\omega)}{2\pi} \int_s \frac{\exp(ikr)}{r} ds \tag{1}$$

where ω is the angular frequency, p_1 is the density of the medium, $V_0(\omega)$ is the normal velocity of the particles on the probe surface, and r is the distance between any point on the probe surface and the position x of the medium. The extended multivariate Gaussian sound beam model can calculate the radiated sound field $P_n(x,\omega)$ of the n array unit through the superposition of 2-D Gaussian sound beams. The expression can be written as:

$$p_n(x,\omega) = v_0(\omega)[\sum_{m=1}^{10} A_m \xi_1(x,z_\omega)] \cdot [\sum_{m=1}^{10} A_m \xi_1(y,z_\omega)] \tag{2}$$

where A_m are 10 complex constants. Following Huygens' principle, the total sound field of an ultrasonic transducer array with N elements can be calculated by superimposing each array element. The sound pressure of a linear phased-array transducer can be written as:

$$p(x,\omega) = \sum_{n=0}^{N-1} p_n(x,\omega) \exp(j\omega t_n) \tag{3}$$

MGB can not only be used to simulate the emission sound field of the piston and rectangular ultrasonic array transducer, but also be used to simulate the propagation

of a sound field in a heterogeneous anisotropic medium and irregular interface and the waveform conversion in the propagation process. In 2003, Ding et al. [13] proposed to calculate the radiated sound field of a rectangular sensor by the superposition of 2-D Gaussian sound beams. This model is called the extended multi-Gaussian beam method (EMGB). However, when EMGB technology is applied to ultrasonic arrays, since it needs to rely on paraxial approximation, modeling errors will occur when the steering angle is greater than about 20 degrees. In 2007, Huang et al. proposed a new multi-Gaussian beam model, called the linear phase multi-Gaussian beam model (LMGB), and proved that it could eliminate these steering angle restrictions. In the 2010s, Han et al. [14] calculated the radiated sound field distribution of an ultrasonic arrays probe with a wedge shape by using the extended multi-Gaussian beam model and measured the ultrasonic arrays probe with an incident angle greater than 10° (refractive angle greater than 20°). The results are modified to enlarge the deflection range of the sound field calculation and the application range of the Gaussian superposition method. In 2019, Anand et al. [15] compared the simulation results of beam propagation through austenitic steel using ordinary multi-Gaussian beam (OMGB) and LMGB models at different steering angles and found that, especially in anisotropic media, the LMGB method was superior to the OMGB method when the steering angle of the beam was greater than 20°. Subsequently, MGB was extended to 3-D ultrasonic sound field simulation [16] and applied to the sound field calculation of complex structural materials and components [17].

2.3. Ray-Tracing Method

The propagation path of sound lines in the workpiece is related to the design of testing technology and the verification of testing ability in the detection process of ultrasonic arrays. The ray-tracing method calculates the propagation path and amplitude attenuation of sound lines in the medium to obtain the propagation state of sound lines in the medium [18]. This method is often used to simulate sound propagation in heterogeneous anisotropic media. The process can be divided into three steps: (1) Solving the equation of elastic wave motion in an anisotropic medium, obtaining the direction of energy velocity and particle displacement. (2) Walking a distance along the direction of energy velocity, the heterogeneous medium is divided into homogeneous regions and the appropriate boundary conditions are given. (3) Calculating the reflected and refracted sound lines on the boundary, and using the boundary conditions to calculate the amplitude of the reflected and refracted sound lines.

The method moved from theory to research applications in 1985 when Ogilvy [19] first proposed a ray-tracing formulation applied to anisotropic nonhomogeneous media in the field. Subsequently, Schmitz et al. applied Ogilvy's Raytraim to the 3-D situation. In the 1990s, Harker et al. [20] verified Raytraim's results by comparing them with the simulation results of the finite difference method. The above studies are based on the basic ray tracing pattern shown in Figure 3a [21]. The marching strategy can also be applied to achieve P2P ray-tracing of Figure 3b when combined with the binary searching algorithm Therefore, P2M ray tracing based on the Dijkstra algorithm is introduced, as shown in Figure 3c. In 2012, Kolkoori et al. [22] presented an adapted 2-D ray-tracing model for evaluating ultrasonic wave fields quantitatively in inhomogeneous anisotropic materials. In 2015, Nowers et al. [23] proposed the fast ray-tracing algorithm to calculate the ultrasonic path through the anisotropic distribution of the predetermined weld seam calculation of the scattering response for a given defect using an effective FEM. In 2018, combining the minimizing and the ray-tracing strategies of marching, an efficient ray-tracing algorithm for ultrasonic array imaging was proposed; the proposed algorithm could realize good imaging performance for defect locating [21].

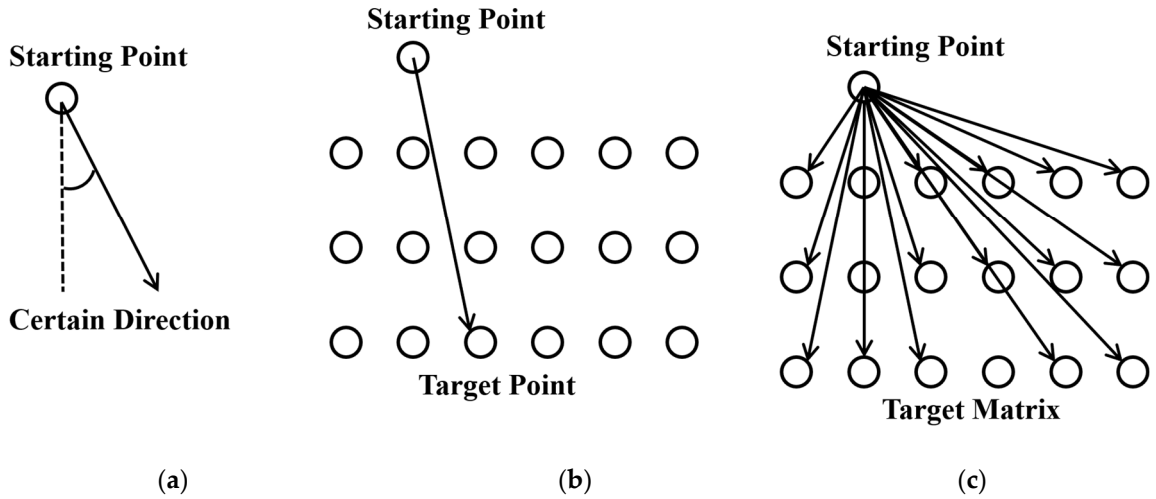


Figure 3. Pathfinding mode. (**a**) Basic mode; (**b**) P2P mode; (**c**) P2M mode.

Several of the above analytical methods can only be used for the simplest geometrical figures. The numerical method can solve the problem of finding a transducer transmitting signal from any shape defect of any shape part. The numerical method is a global discrete approximation method that can solve various complex FEM and FDM problems. Both of these numerical techniques are potential candidates for this task.

2.4. Finite Element Method

FEM was proposed in the 1950s. It is an effective approximate calculation method and is widely used in the field of engineering calculation. FEM analysis divides the object into a finite number of cells. The cells are regarded as under a formation of rigid bodies connected through a finite number of nodes. The force between the elements is transferred through the nodes, and then each unit matrix is established based on the energy principle. After inputting boundary conditions such as loads and constraints, the computer is used to calculate and analyze the object characteristics [24]. At present, the FEM analysis software is ANSYS software [25,26]. The finite element analysis of ultrasonic arrays sound field using ANSYS software is generally divided into the following four steps, as shown in Figure 4.

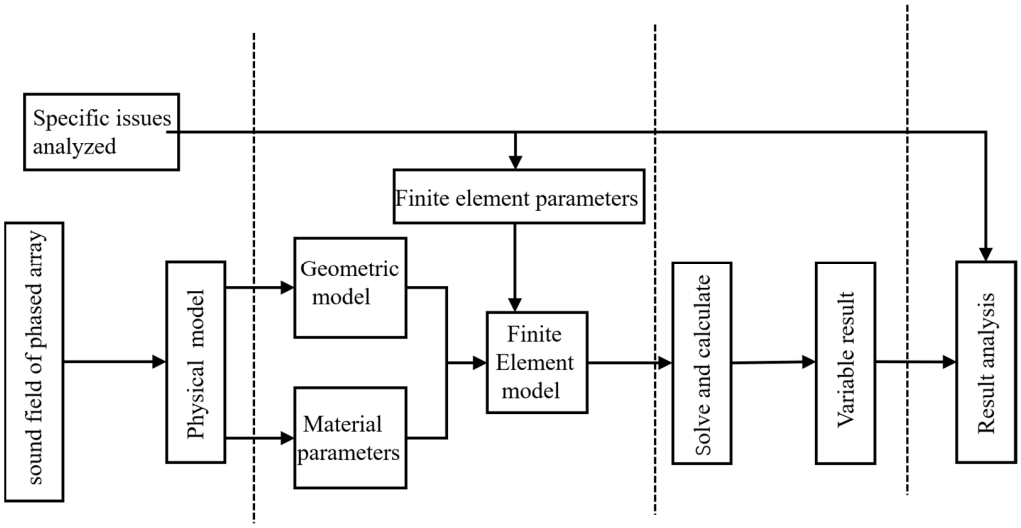


Figure 4. The file chart of ANSYS finite element sound field simulation.

In 1994, Lerch et al. [27] used FEM to carry out an accurate computer simulation of complex ultrasonic transducers, but how to generate planar ultrasonic wave sources with arbitrary incident angles on a given defect is a difficult problem for FEM. Hayashi et al. [28] and Fyleris et al. [29] used semi-analytical FEM to solve the problem of ultrasonic beam focusing when an object with a complex geometric shape propagates. In 2015, Wang et al. [30] used FEM combined with the directivity of metal materials to analyze the focused sound field distribution of an OPFC ultrasonic phased array transducer and found that OPFC material had a broad prospect for the development of ultrasonic array transducers. In 2019, Kim et al. [31] used the commercial finite element software PZ Flex to conduct FEM research in three dimensions and developed two kinds of high-frequency ultrasonic array transducers for specific applications. In the 2020s, Chen et al. [32] studied the ultrasonic time of TOFD ultrasonic array technology FEM used for 2-D geometric material defect detection, established a finite element model through the finite element software ANSYS, compared the error rate between simulation and experiment, and found the feasibility of finite element detection. Because this method needs a large amount of meshing, it requires the high performance of a computer. Currently, FEM is mostly used to simulate 2D thin workpiece detection.

2.5. Finite Difference Method

FDM is a numerical method used to simulate elastic wave propagation [33,34]. In FDM ultrasonic modeling, the propagation medium is divided into staggered grids and probe excitation is applied to the nodes of the corresponding grids in the form of a displacement or stress load. Then, the differential expression is written by the wave equation, and the transient propagation diagram of the sound field at the required time can be calculated. The difference equation can be regarded as the finite approximation of the original equation in terms of a Taylor series expansion. According to the interception method of the Taylor series continuous approximation, the difference scheme can be divided into three kinds:

(1) The Lax-Friedrichs format, explicit, taking three discrete points in space, stable at $|a\Delta t/\Delta x| \leq 1$.

$$\frac{p_k^{n+1} - \left(p_{k+1}^n + p_{k-1}^n\right)/2}{\Delta t} + \frac{a}{\Delta x}\frac{p_{k+1}^n - p_{k-1}^n}{2} = 0 \tag{4}$$

(2) The Leap-Frog format, explicit, taking three discrete points in time, stable at $|a\Delta t/\Delta x| \leq 1$

$$\frac{p_k^{n+1} - p_k^{n-1}}{2\Delta t} + \frac{a}{\Delta x}\frac{p_{k+1}^n - p_{k-1}^n}{2} = 0 \tag{5}$$

(3) The Crank-Nicholson format, implicit, taking three points in space and three points in time.

$$\frac{p_k^{n+1} - p_k^{n-1}}{\Delta t} + \frac{a}{2\Delta x}\left(\frac{p_{k+1}^{n+1} - p_{k-1}^{n+1}}{2} + \frac{p_{k+1}^n - p_{k-1}^n}{2}\right) = 0 \tag{6}$$

where α is the coefficient of the original equation; Δt is the time step; Δx is the space step size; and P is the target value. The finite difference method is commonly used to model the propagation of elastic waves and has three forms of expression: forward, backward, and central differences, which need to be chosen wisely to reduce computational errors. It uses a standard quadrilateral grid, so it is very effective in dealing with regular boundaries, but not as effective as the finite element method for irregular boundaries.

In the 1980s, Liszka et al. [35] presented a modification of the FDM that enables elimination of single or poorly conditioned stars which made local condensation of the grid and the boundary conditions easy to discretize in the case of an arbitrary shape of the domain. In 1996, Balasubramanyam et al. [36] used the finite difference method to simulate

the S0 and A1 Lamb wave modes in a flat metal sheet. The time domain information of the field displacement perpendicular to the group of sheet points is obtained and compared with the Lamb mode dispersion wave. In 2001, Yamawaki et al. [37] used an improved nodal calculation method following fundamental consideration of the elastic wave equations. This improvement is expected to solve the calculation of internal nodes and unified treatment of solid boundaries and applies to composite materials and anisotropic materials. In the literature [38], simulation of the ultrasonic array wave propagation in a 10-mm thick mild-steel pipe specimen has been demonstrated using the FDM method. The simulation results were compared with the experiments of phased array ultrasonic wave interaction with the defects. After 40 years of development, FDM technology has achieved fruitful results in temperature field, flow field simulation, and defect prediction microstructure simulation. A large amount of FDM-based casting process numerical simulation software has emerged, including Magmasoft, AnyCasting, AFSolid, Solidia, NOVCAST, FT-Star, InteCast, CAST soft, etc. [39].

2.6. The Distributed Point Source Method

The analytical method is fast but can only be used for simple cases. The numerical method is widely used but is computationally intensive. To improve the computational speed while ensuring computational accuracy, the semi-analytic method has been proposed. The semi-analytic method is a numerical method that uses a partially analytic solution or analytic function in the calculation process. At present, the semi-analytical method has become the mainstream method for ultrasonic testing simulation and calculation. DPSM is often used to calculate the sound field emitted by the probe using the semi-analytical method. The discrete point source method is usually used to discretize the probe surface into point sources when calculating the sound field emitted by the probe, such as in Rayleigh integration and DPSM [40]. This method uses distributed point sources located slightly below the surface of the transducer to simulate the ultrasonic field. The sound intensity of each point source is obtained by matrix inversion, which requires that the number of target points on the surface of the transducer is equal to the number of point sources. For a rigid baffle-type transducer in a homogeneous medium (as shown in Figure 5), the solution of the linear lossless wave equation can be expressed as a Rayleigh integral [41,42]:

$$p\left(\vec{x},\omega_0\right) = \frac{-j\omega_0 p_0 v_0}{2\pi}\iint_s \frac{e^{jkR}}{R}ds \tag{7}$$

where $p\left(\vec{x},\omega_0\right)$ is the pressure at the field point; ω_0 is the angular frequency; p_0 is the density of the medium; V_0 is the amplitude of the particle velocity that is normal to the transducer surface and distributed uniformly over the entire transducer aperture as $V_z = V_0 e^{-j\omega_0 t}$; t is the time; $k = \omega_0/c$ is the wave number and the velocity of sound in a medium is denoted by c; and R is the distance between the field point and surface element ds.

The transducer is located on the $(x, y, 0)$ plane; ds is the surface element of the transducer; (x, y, z) is the coordinate of the field point $\vec{x}$; R is the distance between the surface element and field point; and the shaded area is the rigid baffle. The purpose is to use M distributed point sources (as shown in Figure 6) to replace the energy device itself to model the ultrasonic field. These point sources are placed on a plane parallel to the surface of the transducer and are slightly offset from the plane r_s. The order of the point source is marked as $1 - M$, the point source and the target point are indexed by m and n, respectively, and the distance between the point source m and the target point n is r_{nm}.

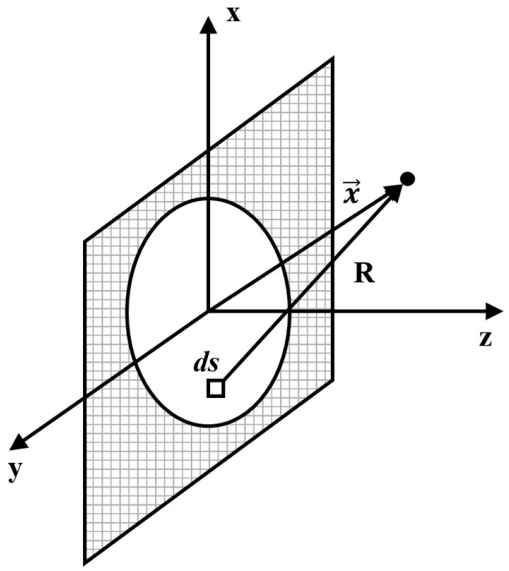


Figure 5. The geometry of the transducer and the field point.

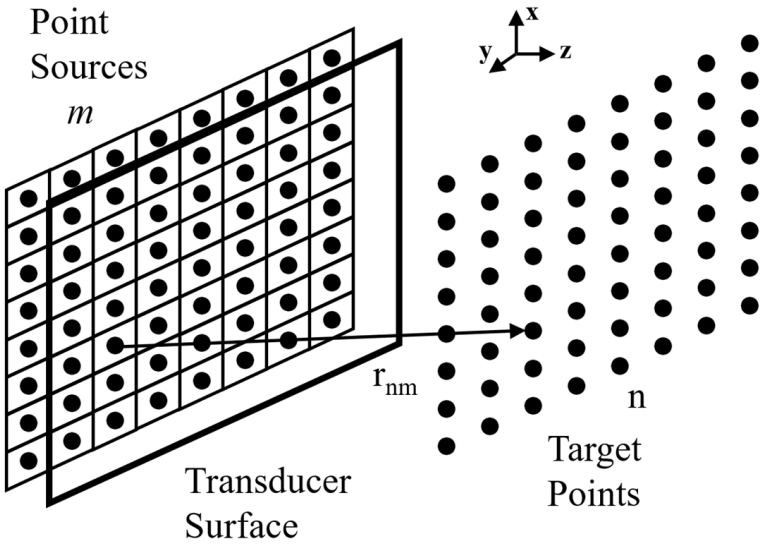


Figure 6. Positioning of distributed point sources, sensor surfaces, and target points.

From this we can simplify the integral summation in Equation (7) and obtain the following equation:

$$p_m\left(\vec{x}, \omega_0\right) = A_m \frac{e^{jkr_m}}{r_m} \tag{8}$$

where m is the index of a point source; r_m is the distance between point source m and field point $\vec{x}$; and $p_m(\vec{x}, \omega_0)$ is the pressure that is contributed by a point source m. $A_m = -j\omega_0 p_0 v_0 ds/2\pi$ is defined as the acoustic intensity of the point source m.

Wooh found in 1998 that the effect of element size on steering characteristics was small and the simple solution obtained by the discrete point source method was very close to that of the phased array. This gives an idea of using the discrete point source method in the ultrasonic arrays [42]. In 2005, Ahmad et al. [43] of the University of Arizona used the DPSM to model the ultrasonic field generated by ultrasonic array transducers and studied the interaction of two-phased array transducers placed in a homogeneous fluid. In 2011, Cheng et al. [44] further extended the DPSM and proposed to solve the least-squares minimization problem by calculating the sound intensity of point sources

without using the traditional matrix iterative method. In the same year, Rahani et al. [45] proposed the Gaussian distributed point source method (G-DPSM) and the elemental source method (ESM), which further optimized the DPSM. Thereafter, the DPSM has been applied in complex problem solving of scalar wave scattering from rough surfaces [46] and in the analysis of ultrasonic fields generated by multiple finite-size ultrasonic transducers in multilayer fluid systems [47].

3. Imaging Technology

Ultrasonic phased-array imaging technology has obvious advantages, and with its application in industrial inspection, traditional fixed-point focus imaging [48,49], as well as dynamic focus imaging [50,51] have shown shortcomings in imaging quality. Therefore, improving the quality of ultrasound imaging and promoting the rapid development of ultrasound imaging in the direction of quantitative detection has been the focus of research. The theory and application of TFM, CSI, and ANI technology are described, which has received much attention from scholars in recent years.

3.1. Total Focusing Method

In 2005, Holmes and others [52] from the University of Bristol in the UK proposed TFM, which caused a sensation in the field of ultrasound imaging research. Under the evaluation coefficient criteria of the array performance indicator (API), the TFM exhibits excellent resolution compared with conventional ultrasonic arrays imaging, which is called the "golden rule" algorithm in ultrasonic arrays technology by some researchers. The data basis for TFM is full matrix capture (FMC). FMC is the most active and efficient of all data acquisition methods because it records the complete set of signals associated with all transmitting and receiving wafers in the array. The FMC process needs to excite each wafer one by one and record the signals received by all the wafers each time. This is shown in Figure 7.

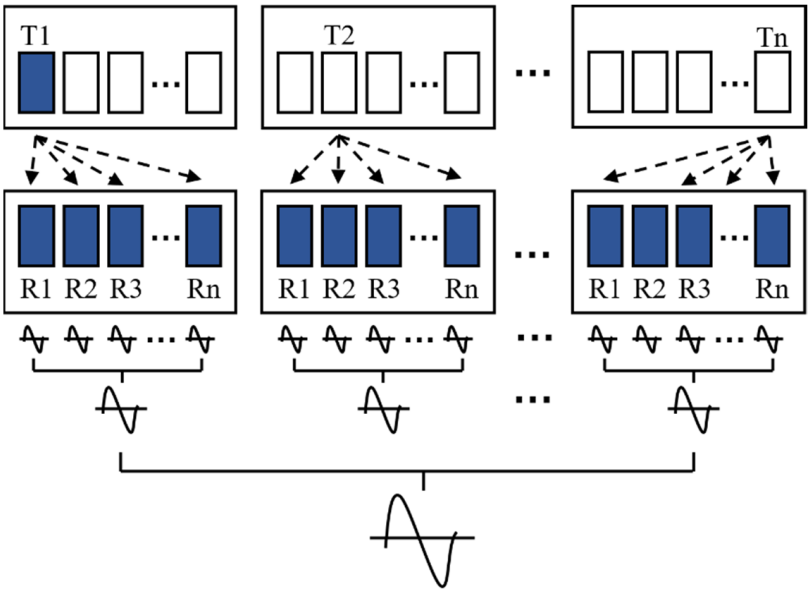


Figure 7. The schematic of the full matrix capture.

Figure 8 is a schematic diagram of FMC reconstruction imaging. After obtaining the full matrix data, a region of interest (ROI) is set in the workpiece and the ROI contains many pixels, i.e., the signal focus. The image amplitude at the point is obtained by delay matching and superposing the echo signal for each transmitting and receiving array element pair. By

traversing each focal point in the ROI, a 2-D reconstructed image is obtained. Taking the point (x, z) as an example, the amplitude $I(x, z)$ at this point should be expressed as:

$$I(x,z) = \sum_{i=1}^{N} \sum_{j=1}^{N} e_{xi,xj}[t_{i,j}(x,z)] \tag{9}$$

where $e_{xi,xj}[t_{i,j}(x,z)]$ is the amplitude of the ultrasonic signal transmitted by the I element and received by the j element superimposed to the position (x, z) and $t_{i,j}(x,z)$ is the delay time required for the sound wave to be emitted from the array element i to the focal point (x, z) and to return from that point to array element j. $t_{i,j}(x,z)$ can be expressed as

$$t_{i,j}(x,z) = \frac{\sqrt{(x-x_i)^2+z^2} + \sqrt{(x-x_j)^2+z^2}}{c} \tag{10}$$

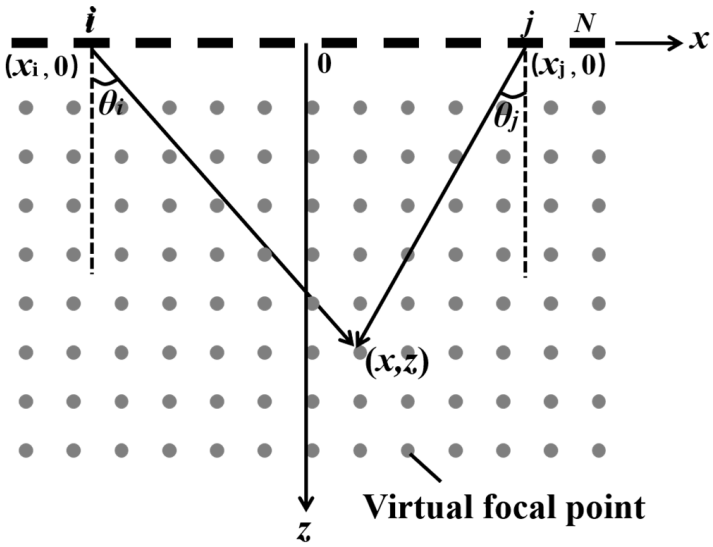


Figure 8. The schematic of the total focusing method.

In the formula, i_x and j_x are the abscissas of the transmitting array element and the receiving array element, respectively, and c is the longitudinal wave velocity of the ultrasonic propagating in the test block.

Considering the amplitude attenuation and deflection of the acoustic beam during propagation, Wilcox et al. [53] proposed two modified TFMs in 2007. The first algorithm for obtaining information about reflector orientation and the second algorithm for distinguishing between point-like reflectors that reflect uniformly in all directions and specular reflectors that have distinct orientations. Since then, Moreau et al. proposed a far-field approximate common-source method (CSM) based on sparse arrays [54,55]. The TFM algorithm has become the golden rule for post-processing algorithms [56–58]. How to effectively sparse optimize and perform weight assignment of ultrasound arrays to achieve better imaging and smaller data volume, as well as how to accelerate full-focus processing and computing, is the focus of current research by scholars in various countries. Hunter et al. [59] introduced the wavenumber algorithm from ultrasonic array radar to improve the computational efficiency of TFM from the frequency domain perspective. However, the wavenumber algorithm has stricter mathematical limitations than TFM, the implementation process is complex, and the selected frequency domain interpolation function can greatly affect the imaging quality. A sparse array FMC based on a particle swarm algorithm was proposed, which can significantly reduce the amount of imaging data while ensuring imaging quality [60]. In the literature [61], an imaging correction model was developed based on an array element directivity function based on a triangular

matrix data acquisition and indexing technique for imaging acceleration algorithm to reduce the imaging time per frame to within 135 ms. Sutcliffe et al. [62] reported that the synthetic aperture total focusing method (SATFM) can achieve higher resolution, but the imaging detection efficiency and real-time performance were not satisfactory. Later, the synthetic aperture method of Virtual Source Aperture (VSA) was proposed. The VSA not only increases the processing speed exponentially, but also maintains good lateral resolution and signal-to-noise ratio by comparing the processing speed parameters of the FMC/TFM, the SATFM [63,64], and the VSA method [65]. The artificial defects of complex welding materials were detected and evaluated successfully using TFM [66–68], and the influence of thickness and material attenuation on volumetric inspection was researched using conventional and advanced TFM-based ultrasonic arrays [69].

Currently, The Eddyfi M2M Gekko ultrasonic flaw detector is a field-proven flaw detector that offers conventional UT, standards.PAUT, TOFD, and real-time TFM. [70]. With the improvement of industrial inspection requirements, 2-D imaging has been fully developed into 3-D imaging; the 3-D method has gradually become the current research hot spot of ultrasonic arrays [71]. Lane et al. [72] used matrix transducers to conduct 1 TFM imaging of the internal defects of structural parts, which can realize 3-D imaging of internal defects without moving the transducer. Given the high price of the 2-D transducer, some researchers [73,74] also use a 1-D linear array transducer to achieve 3-D TFM. TFM is at a critical stage of development; with the further increase in computer speed and acceleration algorithms, the advantages of the FMC data algorithm need to be fully exploited to construct detection and evaluation systems with fast and efficient simulation tools, high IO throughput acquisition units and a large-scale database of theoretical scattering coefficient matrices.

3.2. Compressed Sensing of Array Imaging

The widespread use of ultrasonic array 2-D transducers and the in-depth study of FMC-TFM increase the cost of data capture time and storage space. There is an urgent need to achieve less sampling and real-time detection of data while ensuring the accuracy and validity of the original information [75]. Compressed sensing (CS) is a method for recovering compressed signals from far fewer samples than required by the Nyquist sampling model. The theory was first proposed in 2004 by Candès et al. [76–79], who demonstrated in principle that subsampling can be performed when the signal is sparse and that the original signal can be efficiently reconstructed to reduce the amount of data to be acquired and stored. This method has become a major direction of research in ultrasound array imaging. Figure 9 shows the principal diagram of ultrasonic imaging based on CS. Taking the center of the array as the origin of the component coordinate system, assuming Nx and Ny are the number of scattering points in the horizontal X direction and vertical Y direction, respectively, the received signal can be obtained according to the relevant information as per [80,81].

$$u(r_0, t) = \sum_{i=1}^{I} A(r, t) \cdot \sigma(r_i)$$

$$A(r, t) = \sum_{i=1}^{N} p(r_i, t) = \sum_{i=1}^{N} j e^{j}(\omega t - k r_i) f(\theta_i) = \sqrt{a^2 + b^2} \cdot e^{j(\omega t + \psi)} = E \cdot e^{j(\omega t + \psi)} \quad (11)$$

where $I - N_x N_y$ is the total number of array elements, $p(r, t)$ is the radiated sound field distribution of each array element $E - \sqrt{(a^2 + b^2)}$, $a = \sum_{i=1}^{I} f(\theta_i) \cos(k r_i)$, and $b = \sum_{i=1}^{I} f(\theta) \sin(k r_i)$.

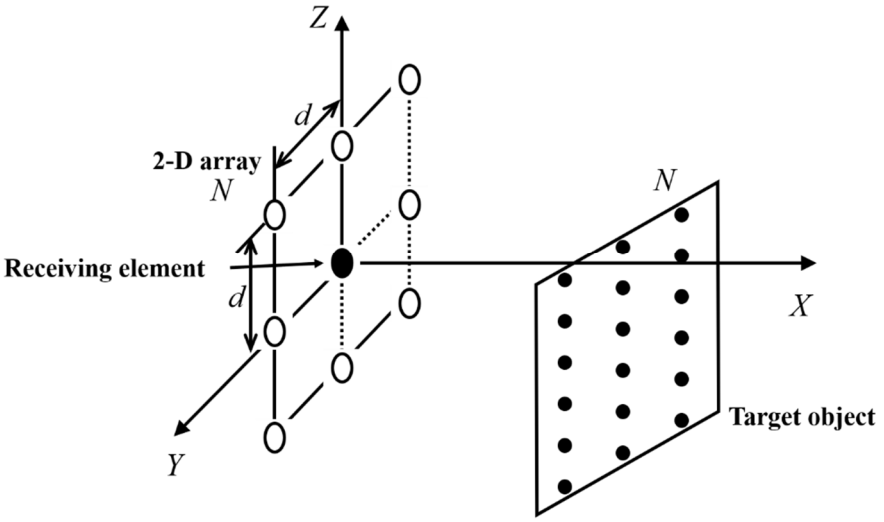


Figure 9. Schematic diagram of ultrasonic arrays imaging based on compressed sensing.

$f(\theta)$ is the directivity function, θ is the angle between the observation point and the Z-axis, r_i is the distance from the i th array element to the observation, $\sigma(r)$ is the transmission coefficient at the midpoint p of the target object, Ψ is the initial phase, and $A(r, t)$ is the sound field distribution at a point. $u(r, t)$ is the distribution of the sound field received by the probe from the target object. For the case of the same received element, the echo function is discretized and sampled at different time nodes to obtain the scattered sound field from the target object:

$$\begin{pmatrix} u(r_0,t_1) \\ u(r_0,t_2) \\ \vdots \\ u(r_0,t_3) \end{pmatrix} = \begin{bmatrix} A(r_1,t_1) & A(r_2,t_1) & \cdots & A\left(r_{N_xN_y},t_1\right) \\ A(r_1,t_2) & A(r_2,t_2) & \cdots & A\left(r_{NxNy},t_2\right) \\ \vdots & \vdots & \ddots & \vdots \\ A(r_1,t_M) & A(r_2,t_M) & \cdots & A\left(r_{N_xN_y},t_M\right) \end{bmatrix} \cdot \begin{bmatrix} \sigma(r_1) \\ \sigma(r_2) \\ \vdots \\ \sigma\left(r_{N_xN_y}\right) \end{bmatrix} \tag{12}$$

Constructing the observation matrix $A(r, t)$ of Equation (12) as a non-singular matrix, the value $\sigma(r_1), \sigma(r_2) \cdots \sigma(r_{N_xN_y})$ after M modulations is obtained, that is, the image information. When $M < N_xN_y$ Equation (12) can be simplified to:

$$U = A \cdot \sigma \tag{13}$$

where U represents the discretized received signal; σ represents the target scene information; and A is the measurement matrix. Considering the effect of noise e in the reception process, the ultrasound imaging model based on compression perception becomes:

$$\min\|\sigma\|_0 s.t. \|A \cdot \sigma - U\|_2^2 \leq \varepsilon \tag{14}$$

CS theory consists of three main elements: the sparse representation of the signal, the compressive measurement process, and the signal reconstruction. Since compressive sensing first transforms the signal to be recovered into a certain sparse domain, the sparse coefficients of the signal in the sparse domain directly determine the reconstruction effect. Currently, designing a high-performance sparse dictionary to guarantee reconstructed images at low compression rates is an attractive research direction. These are major directions to study the method of ultrasonic signal reconstruction based on a sparse dictionary and to analyze the influence of the type of sparse transformation basis on the reconstruction error. Lv et al. [82] used the Fourier basis as the sparse transform basis to reduce the number of receive channels and the amount of data required for imaging using the sparse dictionary technique. Secondly, the design of the measurement matrix is the

key to the successful implementation of CS theory. A method is proposed to obtain the optimal measurement matrix type for phased array ultrasonic beam compression reconstruction by optimizing the incoherence and column independence of the measurement matrix. The acquisition process of a compressed sensing ultrasonic array signal is shown in Figure 10 [83]. Azimipanah et al. [84] performed incoherent compressive sensing (IncCS) and multiple-measurement-vector (MMV)-based compressive sensing reconstruction of the frequency domain data of aluminum block side borehole images acquired by ultrasonic arrays, respectively. The design of reconstruction algorithms is the core of CS theory. The current reconstruction algorithms can be divided into three categories: convex optimization methods, greedy algorithms, and combinatorial algorithms. Bai et al. [85–87] proposed a greedy-algorithm-based CS for ultrasonic array signals. In the literature [88], an experimental system is developed for eight-array sparse sampling based on ultrasonic array techniques and CS. Pyle et al. [89] found that both compressed sensing and wavelet threshold approaches hold promise for achieving large amounts of compression. Although wavelet transformation can improve the signal-to-noise ratio and reconstruction accuracy, CS can be better. To reduce the amount of calculation in the compression process. Wu et al. [90] proposed a CS-based method for reconstructing ultrasonic array FMC data. This method can realize the reconstruction of ultrasonic full-matrix data under a 75% compression rate. The root–means–square error between the reconstructed data and the actual full matrix data is about 6%.

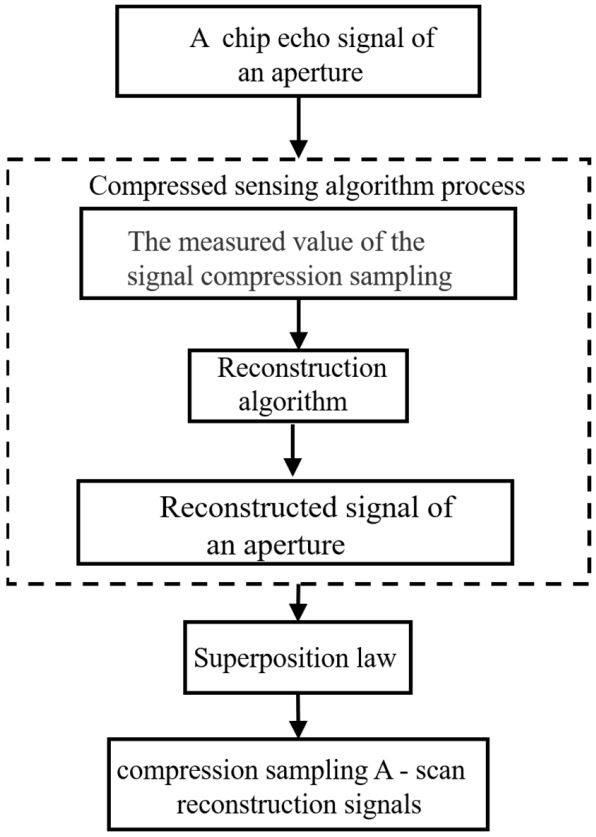


Figure 10. Compressed sensing (CS) of the ultrasonic arrays signals acquisition.

3.3. Nonlinear Ultrasonic Array Imaging

Acoustic nonlinearity imaging has been a hot topic of research since the 1960s [91]. Currently, imaging often uses linear macroscopic defect signals, which are insensitive to defects such as macro-defects and microcracks in materials or structures. In recent years, researchers have performed ultrasonic arrays based on the nonlinear effects of ultrasound to overcome the shortcomings of linear ultrasonic array techniques. The nonlinear acoustic

imaging signals originate from two categories: classical acoustic nonlinearity and contact acoustic nonlinearity [92]. Classical acoustic nonlinearities are concerned with elastic wave distortion due to nonlinearities in the grain structure of materials, while contact acoustic nonlinearity focuses on the study of anomalous acoustic responses caused by the interaction of microscopic or macroscopic defects in the medium with ultrasound waves [93–95]. Among them, contact acoustic nonlinearity has promising applications in material characterization and non-destructive testing [96]. Contact acoustic nonlinearity imaging is divided into harmonic imaging and frequency-modulated imaging.

3.3.1. Harmonic Imaging

The concept of harmonic imaging was first proposed by Averkiou et al. in 1997 [97]. When a continuous pulse train is used to excite large-amplitude ultrasonic waves, it can cause forced vibrations at discontinuities inside the material. As the sound waves propagate in the discontinuous area, the area "closes" or "opens" with the sound wave cycle, intensifying the time-domain waveform distortion, and the frequency domain is manifested as the appearance of harmonics. Relevant studies have shown that harmonic imaging technology can effectively reduce the width of the lateral and axial main lobe of the imaging system and reduce the sidelobe level, thereby significantly improving the spatial resolution and contrast resolution of the system, and can reduce the artifacts caused by sidelobes [98,99]. A 1-D plane longitudinal wave propagating along the α-axis can be expressed as a nonlinear wave [100]:

$$u(x,t) = u_1(x,t) + u_2(x,t) + u_3(x,t) + \ldots, \tag{15}$$

where: $u_1(x,t), u_2(x,t), u_3(x,t)$ denotes fundamental, second harmonic, and third harmonics, respectively. Letting the solution of the fundamental wave be b, then:

$$\begin{gathered} u_2(x,t) = \frac{c_2}{8c_1} k^2 A_1^2 ax \cos(2kx - 2\omega t), \\ u_3(x,t) = \frac{1}{24} k^3 \gamma A_1^3 \left(\frac{c_2^2}{c_1^2} - \frac{c_3}{c_1} \right) \beta x \sin(3kx - 3\omega t) + \frac{c_2^2}{32c_1^2} k^4 A_1^3 \gamma x^2 \cos(3kx - 3\omega t), \end{gathered} \tag{16}$$

where c_1 is the second-order elastic constant; c_2 and c_3 are the higher-order elastic constants; A_1 is the fundamental wave amplitude; and α, β, and γ are the contact nonlinearity factors to represent the effect of contact nonlinearity effects of defects within the solid on nonlinear higher harmonics.

There are three main methods of harmonic separation in harmonic imaging technology: RF filtering techniques, pulse inversion techniques, and pulse amplitude modulation techniques [101].

The RF filtering method uses a filter to remove the fundamental components and only retain the harmonic components. When the frequency band of the emitted fundamental signal is controlled narrowly, the resulting second harmonic and fundamental components are separated into their frequency bands. Since ultrasonic array imaging is a broadband system, the nonlinearity of the detection system or the spectral leakage of the emitted signal will be mixed with the harmonic components, making it difficult to effectively separate the nonlinear signal from the overlapping interference. Ohara et al. [102] first proposed subharmonic ultrasonic arrays for crack evaluation (SPACE). His team developed a SPACE imaging device, as shown in Figure 11. To produce images, propagation times along the paths such as A-B-C-D in Figure 11 were calculated and subtracted before the summation of signals received from each element of the array sensor. The device was capable of acquiring sub-harmonic signals, which were used for sub-harmonic phased-array nonlinear imaging of closed cracks. However, a single-array SPACE could image only the vicinity of a transmission focal point (TFP) when the TFP was fixed. Sugawara et al. [103] developed a confocal SPACE that defines multiple TFPs for imaging closed cracks over a wide area. Park et al. [104] proposed a multi-signal classification method (MUSIC) based on subharmonic ultrasonic phased-array nonlinear imaging. A numerical simulation was used to compare the proposed method with a conventional one, and MUSIC give a narrower

beam width. Experiments also demonstrate that MUSIC can improve the resolution of sub-harmonic imaging.

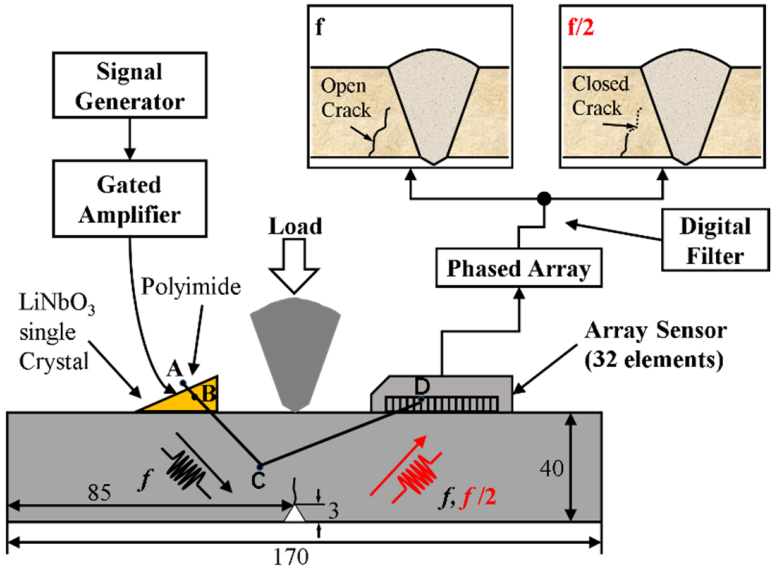


Figure 11. Experimental configuration of a closed-crack imaging method using subharmonic waves. (A is the center position of the $LiNbO_3$ single crystal, B is a passing point on the surface from A to the focal point C, which changes during scanning, and D is the position of an element of the array sensor. A–D is used to calculate propagation time in the specimen and wedge, and a digital bandpass filter is used to extract the fundamental (f) and subharmonic (f/2) components).

Pulsed inversion techniques are an effective method to solve the decrease in system spatial resolution and contrast resolution due to the problems of ultrasonic array broadband systems. It was originally mainly used for acoustic second harmonic imaging in the medical field, which can effectively extract the second harmonic time-domain signal, enhance the amplitude of the second harmonic, and suppress the odd harmonic components mainly generated by the experimental system [105]. Pulsed inversion nonlinear ultrasonic array imaging successively emits positive and negative pulses to obtain the respective A-sweep signals and the signals are sent to the buffer without post-processing after passing through the band-pass filter. At this time, the buffered positive pulse beam is summed with the negative pulse beam to achieve the inverted pulse signal processing. The subsequent signal processing process is identical to that of filter-based nonlinear imaging detection. Peng et al. [106] of Peking University used the non-linear ultrasonic phased array NDT system (Figure 12) to compare and test the detection effects of conventional linear ultrasonic imaging, filtering based nonlinear ultrasonic imaging and pulse inversion nonlinear ultrasonic imaging for tungsten filament phantom. The ultrasound images of the tungsten filament phantom obtained by the three imaging methods are shown in Figure 13. It can be found that the horizontal and axial spatial resolution of pulse inversion nonlinear ultrasonic imaging (PI-NLI) is significantly improved compared with the other two methods.

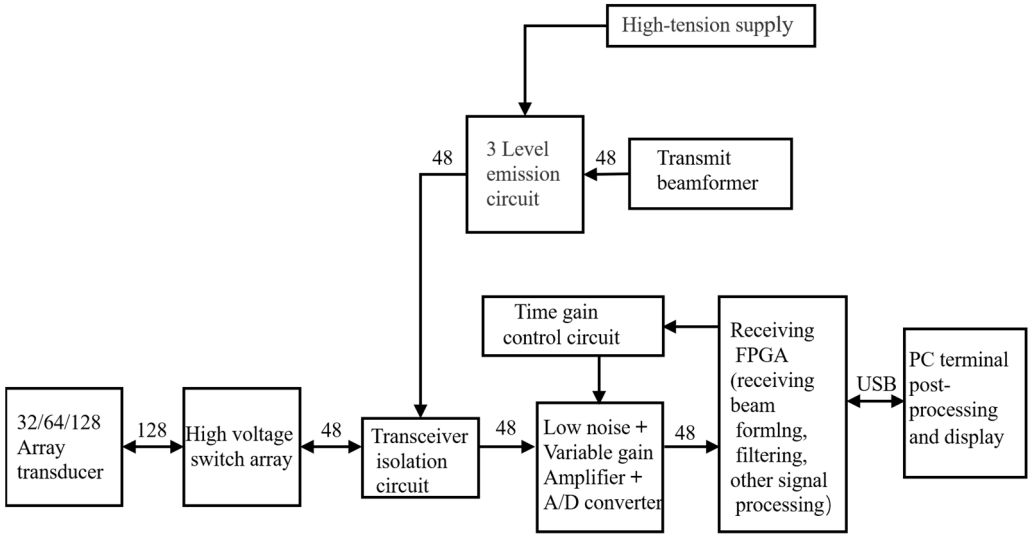


Figure 12. The principal block diagram of the nonlinear ultrasonic arrays NDT system.

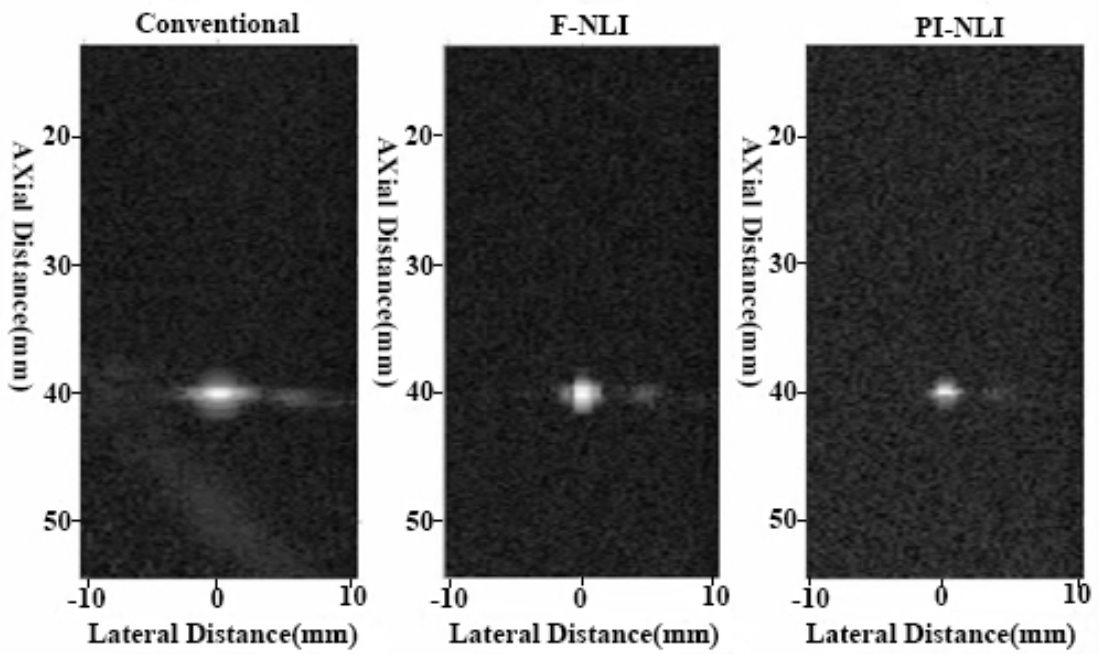


Figure 13. Ultrasonic images of a tungsten filament phantom using conventional ultrasonics/filtering−based nonlinear imaging/pulsed inversion nonlinear imaging methods).

The amplitude modulation technique is to transmit two pulses with different amplitudes and the same phase successively; for example, the latter can be set to be 1/4 of the amplitude of the former one, and then the echo signal generated by the second transmission is multiplied by four and subtracted from the echo generated by the first transmission. Since the amplitude of the second emission is much smaller than the first one, the nonlinear effect is smaller and the harmonic components are not obvious. The fundamental component is canceled and the harmonic component is preserved. Researchers have carried out a large number of nonlinear ultrasonic phased-array imaging detections based on the pulse amplitude modulation method. In [107] a nonlinear ultrasonic imaging method is proposed. This method analyzes the relationship between diffused sound energy, parallel focusing and sequential focusing, and the nonlinear effect under two different phase modes. The results show that the difference of the acoustic energy of two-phase modes within the excitation bandwidth (fundamental wave) can be used as the characteristic parameter for

nonlinear imaging. Based on the nonlinear imaging method using ultrasound arrays in different phase modes, Jiao et al. [108] studied the influence of the time delay and time window for diffuse field sound energy and nonlinear imaging, and the best parameters for nonlinear imaging were obtained when the time delay was 0.67 ms and the time window width ranged from (0.02 ms–0.16 ms). A schematic diagram of nonlinear ultrasonic imaging is shown in Figure 14. The typical result of nonlinear imaging under the best parameters is shown in Figure 15. The authors exploited the energy difference between the different excitation modes for nonlinear ultrasound array imaging. This is shown in Figure 15. Figure 15a shows the distribution of acoustic kinetic energy (Es) of the parallel focusing sound field, and Figure 15b shows the distribution of acoustic kinetic energy (Ep) of the sequential focusing sound field. Neither Figure 15a nor Figure 15b can reflect the existence of microcracks, but the nonlinear imaging obtained from the difference Figure 15c can realize the detection of microcracks.

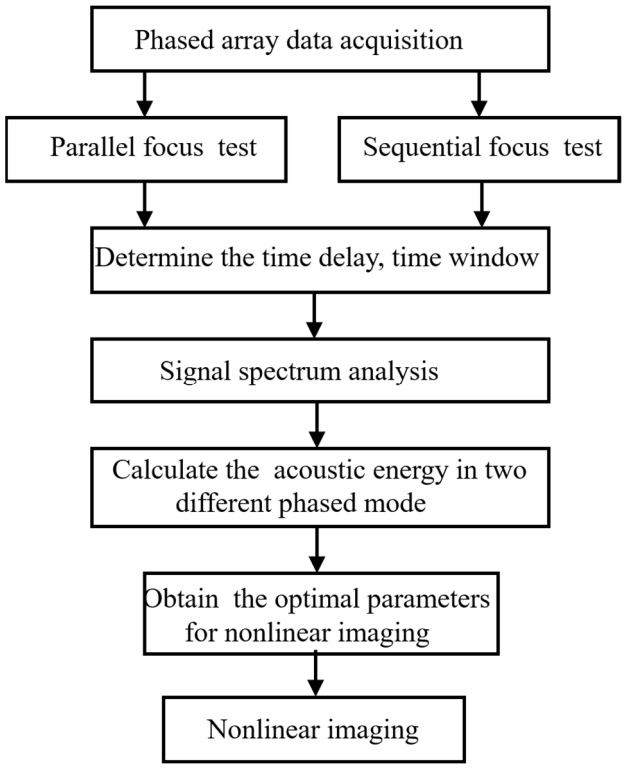


Figure 14. Schematic diagram of nonlinear ultrasonic imaging.

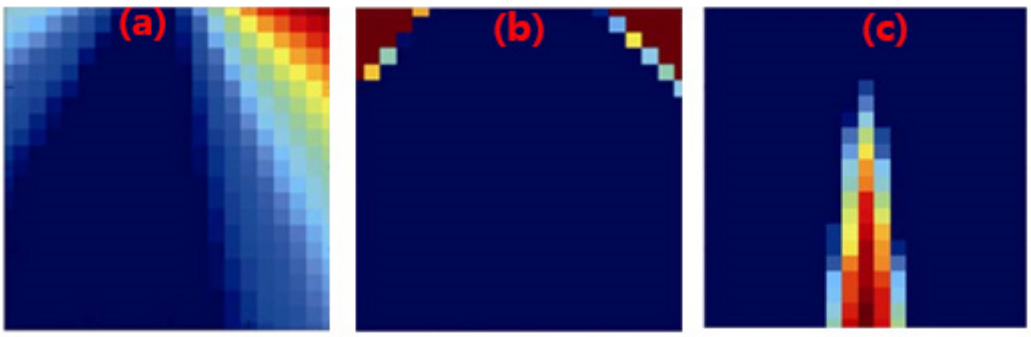


Figure 15. Typical results of nonlinear imaging: (**a**) acoustic energy Es of sequential focusing; (**b**) acoustic energy Ep of parallel focusing; (**c**) sound energy difference between Es and Ep γ (dB).

Haupert et al. [109] proposed an amplitude modulation ultrasonic technique for imaging nonlinear scatterers, such as cracks, buried in a medium. The method consists

of a sequence of three acquisitions for each line of the image. The excitation modes are full-array excitation, odd-numbered array excitation, and even-numbered array excitation. The signals obtained by three excitations are band-pass filtered and signal time-shifted. Then, the full array acquisition signal is used to subtract the sum of the even and odd array acquisition signals to finally obtain the nonlinear signal and perform imaging. Research works show that the AM method reduces temporal resolution (i.e., frame rate) by a factor of three compared to conventional imaging. A schematic of the amplitude modulation technique as shown in Figure 16. Subsequently, the Japanese Ohara et al. [110] investigated the imaging capability of fixed-voltage fundamental wave amplitude difference (fixed-voltage FAD); as a result of applying fixed-voltage FAD with the mechanical scan to the thick and thin specimens, the difference in the crack open/closed distribution was successfully visualized. The results are in good agreement with fracture mechanics. This suggests the usefulness of fixed-voltage FAD not only for NDT for aging infrastructures but also for the progress in fracture mechanics as a new tool.

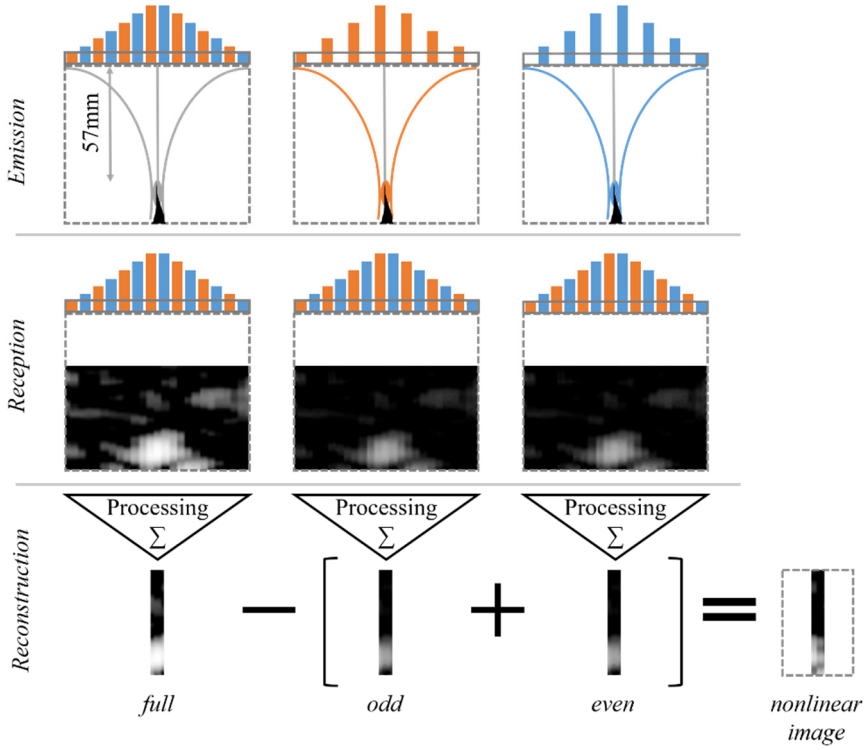


Figure 16. Schematic of the amplitude modulation technique, which consists of a sequence of three acquisitions at the very same focal points with alternative activation of full, odd, or even elements. Signal processing consists of band-pass filtering and time-shifting signals before summation and then subtraction.

3.3.2. Acoustic Modulation Imaging

The acoustic modulation imaging technique uses low frequency (LF) and high frequency (HF) to modulate each other at the crack to generate a para-flop nonlinear signal for performing nonlinear imaging techniques. The schematic of the acoustic modulation is shown in Figure 17. Excite the high-frequency signal and the low-frequency signal into the test piece separately, and the echo signal in the sample without cracks satisfies the linear superposition of the two. On the contrary, the echo signal in the sample with cracks will produce sidelobe signals, which is the modulation signal [111].

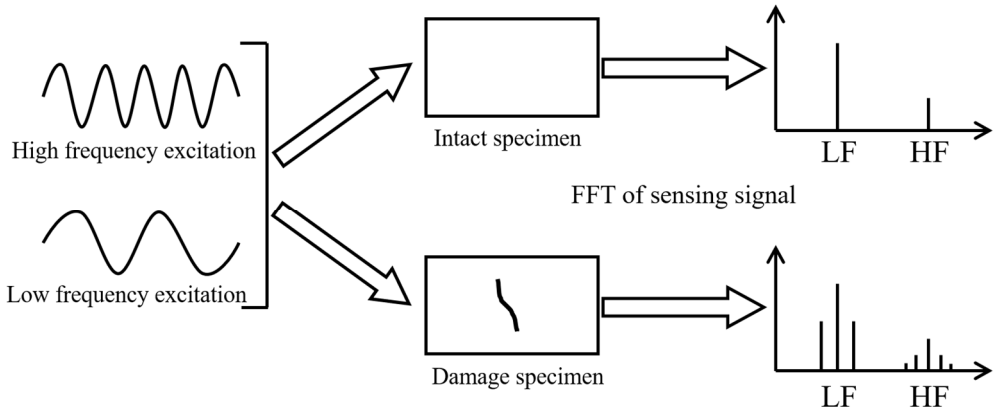


Figure 17. Schematic diagram of sound modulation.

The modulated signal can be expressed in the following form:

$$x_a(t) = A(t)\sin(2\pi f_c t + \varphi_c) \tag{17}$$

$A(t)$ can be expressed by the following equation:

$$A(t) = A[1 + m_a(t)] \tag{18}$$

where $m_a(t)$ is the modulation function equation and A is the amplitude parameter. The amplitude modulation intensity or depth can be defined by the amplitude modulation index as follows:

$$M_a = \frac{m_{\max}}{A} \tag{19}$$

where $m_{\max}$ is the peak value of the signal $m_a(t)$. The modulated signal $X_a(t)$ can be expressed as follows:

$$x_a(t) = A\cos(2\pi f_c t) + \frac{MA}{2}\cos[2\pi(f_c - f_a)t + \varphi] + \frac{MA}{2}\cos[2\pi(f_c + f_a)t + \varphi] \tag{20}$$

where f_c is the main frequency, $f_c - f_a$ is the low-side frequency, and $f_c + f_a$ is the high-side frequency.

In [112,113], it was demonstrated that, for nonlinear acoustic detection of cracks, the modulating effect of the crack-induced vibrations on ultrasonic waves can be used. Kim et al. [114] used low-frequency vibration-modulated pulsed surface waves to detect locally closed fatigue cracks in a specimen and studied the effect of crack size changes on the modulated nonlinear parameters. It was found that the modulated response significantly depended on the ratio of the length of the fatigue crack to the size of the plastic yield zone. Thereafter, an acoustic modulation model was developed [115–117], which can explain the main features observed, to roughly predict the frequency band level obtained by the experiment and select the most suitable acoustic modulation intensity to obtain the best nonlinear modulation signal according to the crack size and the opening and closing states. Ohara et al. [118,119] developed a novel imaging method, subharmonic ultrasonic arrays for crack evaluation (SPACE) based on subharmonic waves and an ultrasonic arrays algorithm, to measure closed-crack depth in the thickness direction.

Although the performance of the SPACE method in closed fatigue and stress corrosion cracks is demonstrated [120], because short-burst input waves might cause filter leakage, objects other than cracks such as coarse grains appear in subharmonic images which might degrade the performance of SPACE for identifying closed cracks. To improve the selectivity of closed cracks for objects other than cracks, a nonlinear ultrasonic imaging method, load difference ultrasonic arrays (LDPA), based on the subtraction of responses at different loads and ultrasonic array techniques, was proposed [121]. A schematic illustration of the

proposed method is shown in Figure 18. By applying external static or dynamic loads to closed cracks, the cracks undergo opening and closing state changes. In contrast, the responses at objects other than crack weld defects were independent of external load. Therefore, the nonlinear signal of the crack can be extracted by subtracting the responses at L1 and L2. The study finds that the LDPA method can perform highly selective imaging of closed cracks in the medium.

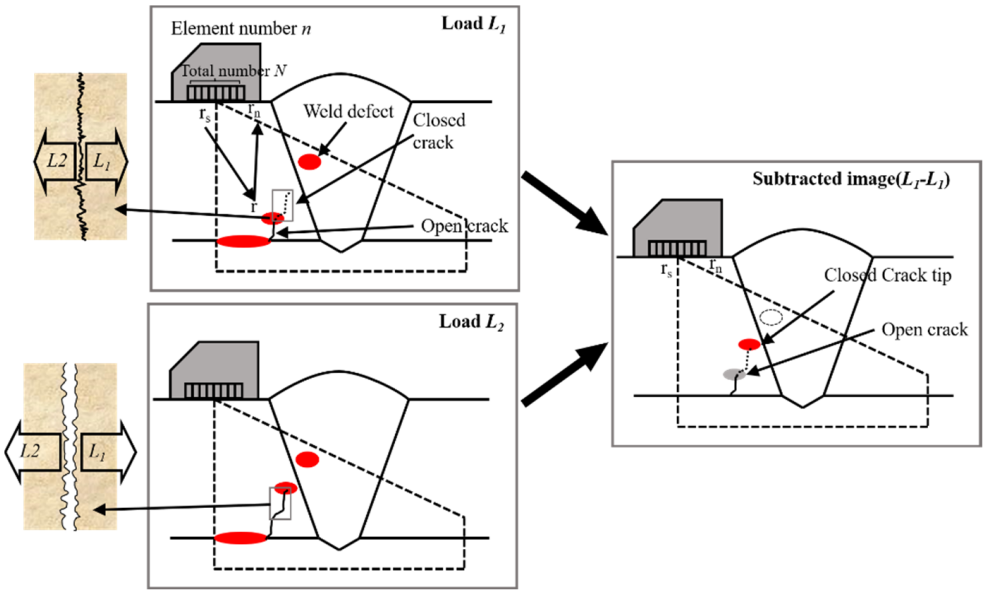


Figure 18. Nonlinear ultrasonic imaging method for closed cracks by subtraction of responses at different loads.

The LDPA nonlinear system uses heavy-duty servo-hydraulic equipment, which increases the weight and volume of the entire system and is not practical. In the literature [122], a crack opening method (GPLC) that combined global preheating (GP) and local cooling (LC) was proposed. This approach could readily increase the tensile thermal stress applied to closed cracks. It has been proven that the combination of GPLC and LDPA10 was useful in selectively imaging closed cracks. Since the availability of the SPACE measurement is limited to only closed cracks and its acoustic energy is weak, this limits the industrial application of this method. Mihara el at. [123] combined a high-voltage transformer with a low-cost pulse and synthetic aperture and digital filtering post-processing technology to develop a new SPACE system for wider industrial inspection fields. The improved commercial ultrasonic array system is shown in Figure 19. In addition, an ultrasonic array micro-crack nonlinear positioning imaging method that combines vibrating acoustic modulation technology and a time-delay superposition algorithm is proposed [124].

Jiao et al. [125] used sparsely distributed sensors to extract the nonlinear response at the vibration frequency and used it for defect imaging. Research shows that the nonlinear guided wave excitation method based on vibration modulation can effectively characterize and locate nonlinear contact defects. The diagram of the vibration-modulated ultrasonic guided wave detection system is shown in Figure 20.

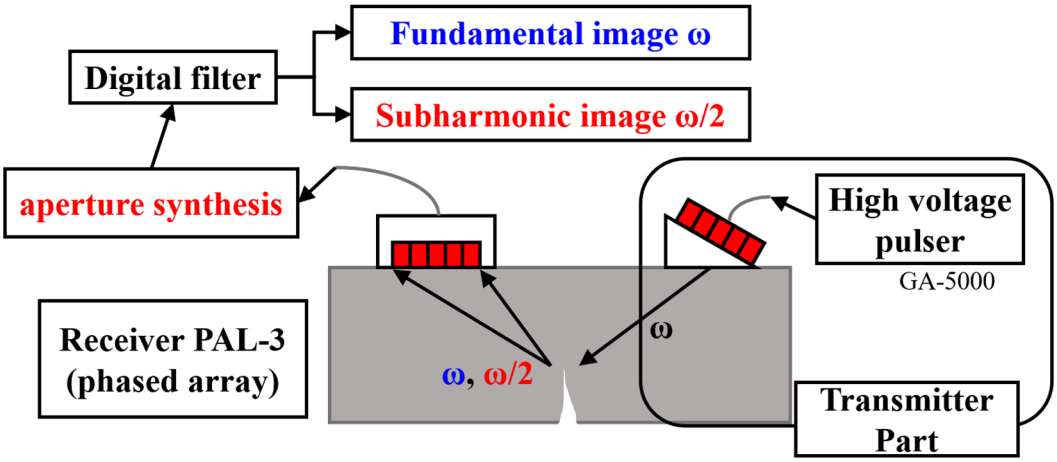


Figure 19. Schematic diagram of conventional SPACE.

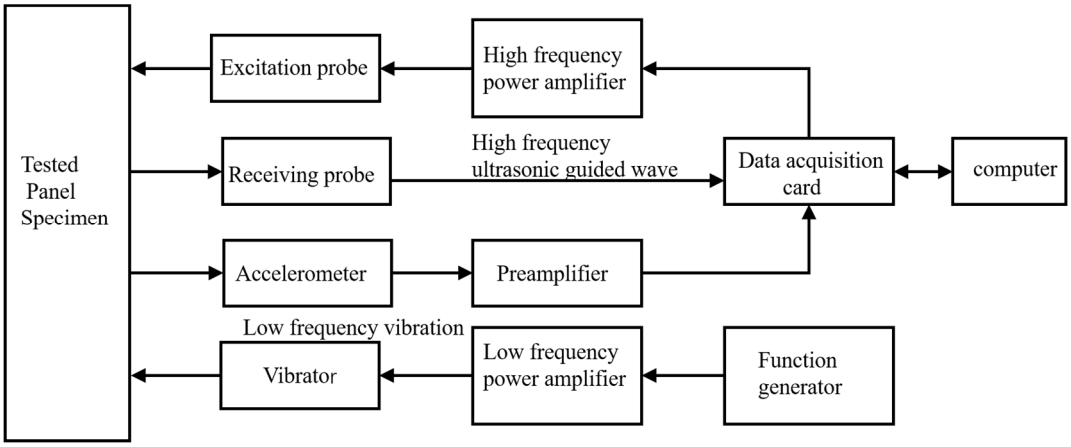


Figure 20. The diagram of the vibration-modulated ultrasonic guided wave detection system.

4. Conclusions

This paper has reviewed current research progress in the common modeling methods and the imaging methods of ultrasonic arrays which have attracted much attention. It can be seen that the development direction of ultrasonic arrays must be quantitative and improve the detection reliability as the goal.

(1) These modeling methods need to be performed as part of the ultrasonic arrays inspection development process. From a macroscopic point of view, NDE has become part of information technology, ultrasonic acoustic field calculation, and analysis simulation that, based on quantitative and digital plays a crucial part in the use of ultrasonic arrays. This section reviews the basic theories of the different modeling methods and the application of these methods in ultrasonic arrays. The unique advantages of different modeling methods are discussed, including modeling the sound field generated by any probe, the emission and transmission of the sound field at any complex interface, and the propagation of the sound field in anisotropic media, multilayer media, and heterogeneous media. However, there are still some problems that need to be further studied in the future: (1) the sound-field-modeling method of adaptive arrays is not mature, and there are many arrays and probe shapes. For different types of transducers, the modeling process and results are different, which increases the modeling workload. (2) It is difficult to model sound fields in complex environments such as heterogeneous media and laminated structures.

(2) TFM is a major research focus in NDT and still facing the following challenges: (1) The influence of defect scattering on TFM is worth further study. Getting defect scattering of the main energy is the key to high-resolution TFM, but, at present, only some

defect scattering information is collected by the transducer. Therefore, obtaining as much complete defect scattering information as possible is the key to improving TFM accuracy and accurate qualitative and quantitative analysis of defects, which is also the development direction of defect qualitative and quantitative analysis. (2) Massive data and complex data processing work has been brought along with the gradual application of 3-D imaging inspection methods with 2-D transducers. This not only increases the cost of the ultrasonic array hardware system but also increases the volume and weight of the equipment. Therefore, a fast and efficient simulation tool, a high IO throughput acquisition unit, and an inspection evaluation system need to be built as soon as possible. The aim is to achieve better high-resolution 3-D imaging and real-time imaging for industrial inspection. In summary, the current TFM still needs more in-depth research in the areas of imaging accuracy, qualitative and quantitative analysis of defects, 3-D imaging, and real-time imaging.

(3) CS faces challenges in ultrasonic array structure damage detection, firstly how to make faster and more accurate heterogeneous sets of data collected from sensors and extracting information that allows the estimation of the damage condition of a structure. Another important challenge is to explore the unique features of PAUT data, and the extraction of these features and the recognition of sparse data models need further development. More research should focus on sparse representation in the future. In addition, how to collect relevant data from a structure in a cost-effective manner and respect the size, weight, cost, energy consumption, and bandwidth limitations placed on the system also need to be solved.

(4) Vibration, ultrasonic, and acoustic nonlinear phenomena have been used for many years to detect material defects and structural damage. Nonlinear ultrasonic array technology has been in the critical stage of transition from laboratory application to engineering application, from qualitative detection and evaluation to quantitative detection and evaluation, and from characteristic detection of materials and structures to life prediction. The future research focus of nonlinear ultrasonic array technology is mainly to clarify the discontinuous interaction mechanism between acoustic waves and the medium during nonlinear ultrasonic detection and to solve problems such as defect identification and detection robustness. Meanwhile, how to quickly extract useful information from the aspects of experimental method research, signal processing, and imaging is also to be studied. In addition, the nonlinear detection of industrial ultrasonic arrays is more complex than for medical detection environment. The characteristics of objects are more diverse and the interference factors are greater in industrial detection. Therefore, there is still a long way to go in the process of nonlinear acoustic imaging from laboratory research to industrial field application. So far, nonlinear acoustics is still in the development stage and is the most challenging frontier basic research direction in the field of acoustics.

Funding: This research was funded by the Jiangsu Graduate Research and Practice Innovation Program grant number KYCX22_0348 And The APC was funded by Key Laboratory of Non-Destructive Testing and Monitoring Technology for High-Speed Transport Facilities of the Ministry of Industry and Information Technology grant number No. NJ2020014.

Institutional Review Board Statement: Not applicable.

Informed Consent Statement: Informed consent was obtained from all subjects involved in the study.

Acknowledgments: This work was funded by the Jiangsu Graduate Research and Practice Innovation Program [Grant Number KYCX22_0348], Key Laboratory of Non-Destructive Testing and Monitoring Technology for High-Speed Transport Facilities of the Ministry of Industry and Information Technology and the Fundamental Research Funds for the Central Universities, No. NJ2020014.

Conflicts of Interest: The authors declare no conflict of interest.

References

1. Drinkwater, B.W.; Wilcox, P.D. Ultrasonic arrays for non-destructive evaluation: A review. *NDT E Int.* **2006**, *39*, 525–541. [CrossRef]
2. Felice, M.V.; Fan, Z. Sizing of flaws using ultrasonic bulk wave testing: A review. *Ultrasonics* **2018**, *88*, 26–42. [CrossRef] [PubMed]
3. Jin, Y.F. Industry 4.0 and Nondestructive Testing of China. *Nondestruct. Test.* **2016**, *38*, 58–62. (In Chinese)
4. Stevenson, W.H. Optical frequency shifting by means of a rotating diffraction grating. *Appl. Opt.* **1970**, *9*, 649–652. [CrossRef]
5. Kozacki, T.; Falaggis, K.; Kujawinska, M. Computation of diffracted fields for the case of high numerical aperture using the angular spectrum method. *Appl. Opt.* **2012**, *51*, 7080–7088. [CrossRef]
6. Schafer, M.E.; Lewin, P.A. Transducer characterization using the angular spectrum method. *J. Acoust. Soc. Am.* **1989**, *85*, 2202–2214. [CrossRef]
7. Belgroune, D.; de Belleval, J.F.; Djelouah, H. A theoretical study of ultrasonic wave transmission through a fluid-solid interface. *Ultrasonics* **2008**, *48*, 220–230. [CrossRef]
8. Vyas, U.; Christensen, D. Ultrasound beam propagation using the hybrid angular spectrum method. In Proceedings of the 2008 30th Annual International Conference of the IEEE Engineering in Medicine and Biology Society, Vancouver, BC, Canada, 20–25 August 2008; pp. 2526–2529.
9. Vyas, U.; Christensen, D. Ultrasound beam simulations in inhomogeneous tissue geometries using the hybrid angular spectrum method. *IEEE Trans. Ultrason. Ferroelectr. Freq. Control* **2012**, *59*, 1093–1100. [CrossRef]
10. Ilyina, N.; Hermans, J.; Van Den Abeele, K.; D'hooge, J. Extension of the angular spectrum method to model the pressure field of a cylindrically curved array transducer. *J. Acoust. Soc. Am.* **2017**, *141*, EL262–EL266. [CrossRef]
11. Wen, J.J.; Breazeale, M.A. A diffraction beam field expressed as the superposition of Gaussian beams. *J. Acoust. Soc. Am.* **1988**, *83*, 1752–1756. [CrossRef]
12. Schmerr, L.W. *Fundamentals of Ultrasonic Nondestructive Evaluation a Modeling Approach*; Plenum Press: New York, NY, USA; London, UK, 1998.
13. Ding, D.S.; Zhang, Y.; Liu, J.Q. Some extensions of the Gaussian beam expansion: Radiation fields of the rectangular and the elliptical transducer. *J. Acoust. Soc. Am.* **2003**, *113*, 3043–3048. [CrossRef] [PubMed]
14. Han, P.; Wang, Z.B.; Chen, Y.X. Simulation of sound fields of ultrasonic phased array sensor based on multi-Gaussian beam model. *Transducer Microsyst. Technol.* **2010**, *29*, 22–25. (In Chinese)
15. Anand, C.; Delrue, S.; Jeong, H.; Shroff, S.; Groves, R.M.; Benedictus, R. Simulation of ultrasonic beam propagation from phased arrays in anisotropic media using linearly phased multi-Gaussian beams. *IEEE Trans. Ultrason. Ferroelectr. Freq. Control* **2019**, *67*, 106–116. [CrossRef] [PubMed]
16. Guo, W.J.; Chen, Y.X.; Jin, Y.; Wang, Z.B. Sound field simulation of ultrasonic inspection of cylinders based on multi-Gaussian beam model. *Appl. Acoust.* **2013**, *32*, 354–360. (In Chinese)
17. Jiang, X.P.; Han, H.B.; Jia, J.; Zhang, L.; Yue, Y.F. Theoretical study on the characteristics of the sound field radiated by a Gaussian rectangular transducer. In Proceedings of the AOPC 2020: Optics Ultra Precision Manufacturing and Testing, Beijing, China, 30 November–2 December 2020; Volume 11568, p. 115681U.
18. Ye, J.; Kim, H.J.; Song, S.J. Development of an ultrasonic ray model for phased array ultrasonic testing in austenitic weldments. In Proceedings of the 17th World Conference on Nondestructive Testing, Shanghai, China, 25–28 October 2008.
19. Ogilvy, J.A. Computerized ultrasonic ray tracing in austenitic steel. *NDT Int.* **1985**, *18*, 67–77. [CrossRef]
20. Zhao, X.; Song, S.J.; Kim, H.J.; Gang, T.; Kang, S.C.; Choi, Y.H.; Kang, S.S. Determination of incident angle and position of optimal mode ultrasonic beam for flaw detection in anisotropic and inhomogeneous weldments by ray tracing. *J. Korean Soc. Nondestruct. Test.* **2007**, *27*, 231–238.
21. Zhou, H.; Han, Z.; Du, D.; Chen, Y. A combined marching and minimizing ray-tracing algorithm developed for ultrasonic array imaging of austenitic welds. *NDT E Int.* **2018**, *95*, 45–56. [CrossRef]
22. Kolkoori, S.R.; Rahman, M.U.; Chinta, P.K.; Ktreutzbruck, M.; Rethmeier, M.; Prager, J. Ultrasonic field profile evaluation in acoustically inhomogeneous anisotropic materials using 2-D ray-tracing model: Numerical and experimental comparison. *Ultrasonics* **2013**, *53*, 396–411. [CrossRef]
23. Nowers, O.; Duxbury, D.J.; Drinkwater, B.W. Ultrasonic array imaging through an anisotropic austenitic steel weld using an efficient ray-tracing algorithm. *NDT E Int.* **2016**, *79*, 98–108. [CrossRef]
24. Lord, W.; Ludwig, R.; You, Z. Developments in ultrasonic modeling with finite element analysis. *J. Nondestruct. Eval.* **1990**, *9*, 129–143. [CrossRef]
25. Zhang, J.; Drinkwater, B.W.; Wilcox, P.D. Defect characterization using an ultrasonic array to measure the scattering coefficient matrix. *IEEE Trans. Ultrason. Ferroelectr. Freq. Control* **2008**, *55*, 2254–2265. [CrossRef] [PubMed]
26. Xiao, K.F. Numerical Analysis and Photoelasticitic Expert Meant Study of the Ultrasonic Propagation in Solid. Master's Thesis, North University of China, Taiyuan, China, 2008. (In Chinese)
27. Lerch, T.P. *Ultrasonic Transducer Characterization and Transducer Beam Modeling for Applications in Nondestructive Evaluation*; Iowa State University: Ames, IA, USA, 1996.
28. Hayashi, T.; Kawashima, K.; Sun, Z.; Rose, J.L. Analysis of flexural mode focusing by a semianalytical finite element method. *J. Acoust. Soc. Am.* **2003**, *113*, 1241–1248. [CrossRef] [PubMed]
29. Fyleris, T.; Jasiuniene, E. Analytic Approach for 2D Phased Array Delay Law Calculation in Case of Inspection of Objects with Complex Geometry. *Elektron. Elektrotechnika* **2019**, *25*, 28–31. [CrossRef]

30. Wang, Z.; Luo, Y.; Zhao, G.; Yuan, F.G. Design and optimization of an OPFC ultrasonic linear ultrasonic phased array transducer. *Int. J. Mech. Mater. Des.* **2017**, *13*, 57–69. [CrossRef]
31. Kim, J.N. *Closed-Loop Finite Element Design of Array Ultrasonic Transducers for High-Frequency Applications*; The Pennsylvania State University: State College, PA, USA, 2019.
32. Chen, H.; Fan, D.; Huang, J.; Huang, W.; Zhang, G.; Huang, L. Finite element analysis model on ultrasonic phased array technique for material defect time of flight diffraction detection. *Sci. Adv. Mater.* **2020**, *12*, 665–675. [CrossRef]
33. Bond, L.J.; Saffari, N.; Punjani, M. Modeling Ultrasonic Waves Using Finite Difference Methods. In *Review of Progress in Quantitative Nondestructive Evaluation*; Springer: Boston, MA, USA, 1987; Volume 6A, pp. 135–144.
34. Temple, J.A.G. Modelling the propagation and scattering of elastic waves in inhomogeneous anisotropic media. *J. Phys. D Appl. Phys.* **1988**, *21*, 859. [CrossRef]
35. Liszka, T.; Orkisz, J. The finite difference method at arbitrary irregular grids and its application in applied mechanics. *Comput. Struct.* **1980**, *11*, 83–95. [CrossRef]
36. Balasubramanyam, R.; Quinney, D.; Challis, R.E.; Todd CP, D. A finite-difference simulation of ultrasonic Lamb waves in metal sheets with experimental verification. *J. Phys. D Appl. Phys.* **1996**, *29*, 147. [CrossRef]
37. Yamawaki, H.; Saito, T. Numerical calculation of ultrasonic propagation with anisotropy. *NDT E Int.* **2000**, *33*, 489–497. [CrossRef]
38. Alia, A.; Djelouah, H.; Bouaoua, N. Finite difference modeling of the ultrasonic field radiated by circular transducers. *J. Comput. Acoust.* **2004**, *12*, 475–499. [CrossRef]
39. Liao, D.M. Study on Numerical Simulation of Thermal Stresses during Casting's Solidification Process Based on FDM. Ph.D. Thesis, Huazhong University of Science & Technology, Wuhan, China, 2002. (In Chinese).
40. Alnuaimi, N.A. Modeling Ultrasonic Transducer Inhomogeneous and Non-Homogeneous Media Using the DPSM Method. Ph.D. Thesis, The University of Arizona, Tucson, AZ, USA, 2004.
41. Williams, E.G.; Maynard, J.D. Numerical evaluation of the Rayleigh integral for planar radiators using the FFT. *J. Acoust. Soc. Am.* **1982**, *72*, 2020–2030. [CrossRef]
42. Wooh, S.C.; Shi, Y. Influence of ultrasonic phased array element size on beam steering behavior. *Ultrasonics* **1998**, *36*, 737–749. [CrossRef]
43. Ahmad, R.; Kundu, T.; Placko, D. Modeling of ultrasonic phased arraytransducers. *J. Acoust. Soc. Am.* **2005**, *117*, 1762–1776. [CrossRef] [PubMed]
44. Cheng, J.Q.; Wei, L.; Qin, Y.X. Extension of the distributed point source method for ultrasonic field modeling. *Ultrasonics* **2011**, *51*, 571–580. [CrossRef]
45. Rahani, E.K.; Kundu, T. Gaussian-DPSM (G-DPSM) and Element Source Method (ESM) modifications to DPSM for ultrasonic field modeling. *Ultrasonics* **2011**, *51*, 625–631. [CrossRef]
46. Jarvis, A.J.C.; Cegla, F.B. Application of the distributed point source method to rough surface scattering and ultrasonic wall thickness measurement. *J. Acoust. Soc. Am.* **2012**, *132*, 1325–1335. [CrossRef]
47. Vempati, A.S.; Ahmad, R. Ultrasonic Wave Scattering at Liquid-Solid Interface by ultrasonic phased array sensor Using Distributed Point Source Method (DPSM). In *European Workshop on Structural Health Monitoring*; Springer: Cham, Switzerland, 2020; pp. 276–285.
48. Yan, L. Ultrasonicultrasonic phased array technology the first part of the basic concepts. *NDT* **2007**, *31*, 24–28. (In Chinese)
49. Li, Y.; Wang, Z.B.; Zhao, X. The Analysis of Time-delay Precision on the Digitalultrasonicultrasonic phased array testing System. *J. Proj. Rocket. Missiles Guid.* **2008**, *28*, 194–196. (In Chinese)
50. Ma, J.C.; Shen, Y.; Su, B.K. Research evolution of ultrasound beamforming technology. *Chin. J. Med. Instrum.* **2005**, *29*, 438–443.
51. Smith, S.W.; Pavy, H.G.; von Ramm, O.T. High-speed ultrasound volumetric imaging system. I. Transducer design and beam steering. *IEEE Trans. Ultrason. Ferroelectr. Freq. Control* **1991**, *38*, 100–108. [CrossRef]
52. Holmes, C.; Drinkwater, B.W.; Wilcox, P.D. Post-processing of the full matrix of ultrasonic transmit–receive array data for non-destructive evaluation. *NDT E Int.* **2005**, *38*, 701–711. [CrossRef]
53. Wilcox, P.D.; Holmes, C.; Drinkwater, B.W. Advanced reflector characterization with ultrasonic phased arrays in NDE applications. *IEEE Trans. Ultrason. Ferroelectr. Freq. Control* **2007**, *54*, 1541–1550. [CrossRef] [PubMed]
54. Moreau, L.; Drinkwater, B.W.; Wilcox, P.D. Ultrasonic imaging algorithms with limited transmission cycles for rapid nondestructive evaluation. *IEEE Trans. Ultrason. Ferroelectr. Freq. Control* **2009**, *56*, 1932–1944. [CrossRef] [PubMed]
55. Holford, I.K.; Gran, F.; Jensen, J.A. Broadband minimum variance beamforming for ultrasound imaging. *IEEE Trans. Ultrason. Ferroelectr. Freq. Control* **2009**, *56*, 314–325. [CrossRef]
56. Weston, M.; Mudge, P.; Davis, C.; Peyton, A. Time efficient auto-focussing algorithms for ultrasonic inspection of dual-layered media using full matrix capture. *Ndt E International* **2012**, *47*, 43–50. [CrossRef]
57. Mirjalili, S. Genetic algorithm. In *Evolutionary Algorithms and Neural Networks*; Springer: Cham, Switzerland, 2019; pp. 43–55.
58. Ingber, L. Simulated annealing: Practice versus theory. *Math. Comput. Model.* **1993**, *18*, 29–57. [CrossRef]
59. Hunter, A.J.; Drinkwater, B.W.; Wilcox, P.D. The wavenumber algorithm for full-matrix imaging using the ultrasonic phased array. *IEEE Trans. Ultrason. Ferroelectr. Freq. Control* **2008**, *55*, 2450–2462. [CrossRef]
60. Shen, X.W. Ultrasonic sparse-TFM imaging using particle swarm optimization algorithm. *J. Appl. Acoust.* **2020**, *39*, 354–359. (In Chinese)

61. Jia, L.C.; Chen, S.L.; Bai, Z.L.; Zeng, Z.M.; Yang, X.X. Correction model and accelerating algorithm for ultrasonic total focusing method. *Chin. J. Sci. Instrum.* **2017**, *38*, 1589–1596. (In Chinese)
62. Sutcliffe, M.; Weston, M.; Charlton, P.; Dutton, B.; Donne, K. Virtual source aperture imaging for non-destructive testing. *Insight-Non-Destr. Test. Cond. Monit.* **2012**, *54*, 371–379. [CrossRef]
63. Trots, I.; Tasinkevych, Y.; Nowicki, A.; Lewandowski, M. Multi-element synthetic transmit aperture method in medical ultrasound imaging. *Eng. Technol.* **2011**, *80*, 201–206.
64. Yang, J.; Luo, L.; Yang, K.; Zhang, Y. Ultrasonicultrasonic Phased Array Sparse TFM Imaging Based on Virtual Source and Phase Coherent Weighting. *IEEE Access* **2020**, *8*, 185609–185618. [CrossRef]
65. Kumar, A. Ultrasonicultrasonic phased array imaging using angle beam virtual source full matrix capture-total focusing method. *NDT E Int.* **2020**, *116*, 102324.
66. Javadi, Y.; MacLeod, C.N.; Pierce, S.G.; Gachagan, A.; Kerr, W.; Ding, J.; Dziewierz, J. Ultrasonicultrasonic phased array inspection of wire+ arc additive manufacture samples using conventional and total focusing method imaging approaches. *Insight-Non-Destr. Test. Cond. Monit.* **2019**, *61*, 144–148.
67. Camacho, J.; Atehortua, D.; Cruza, J.F.; Brizuela, J.; Ealo, J. Ultrasonic crack evaluation by phase coherence processing and TFM and its application to online monitoring in fatigue tests. *NDT E Int.* **2018**, *93*, 164–174. [CrossRef]
68. Peng, C.Y.; Shen, P.; Wang, Z.X.; Zhang, J. The Evaluation of Ultrasonic FMC/TFM on Real Fatigue Cracks. In Proceedings of the 2019 Far East NDT New Technology & Application Forum (FENDT), Qingdao, China, 24–27 June 2019; pp. 11–15.
69. Ponseenivasan, S.; Kumar, A. Comparative Study on Using Ultrasonic Array-Based Techniques for Detection of Flaws in Thick and Attenuating Materials. *Trans. Indian Inst. Met.* **2021**, *74*, 499–510.
70. Zhang, J.; Drinkwater, B.W.; Wilcox, P.D.; Hunter, A.J. Defect detection using ultrasonic phased arrays: The multi-mode total focusing method. *NDT E Int.* **2010**, *43*, 123–133. [CrossRef]
71. McKee, J.G.; Bevan, R.L.; Wilcox, P.D.; Malkin, R.E. Volumetric imaging through a doubly-curved surface using a 2D phased array. *NDT E Int.* **2020**, *113*, 102260. [CrossRef]
72. Lane CJ, L.; Dunhill, A.K.; Drinkwater, B.W.; Wilcox, P.D. The development of a 2D ultrasonic array system for the in situ inspection of single crystal turbine blades. *AIP Conf. Proc.* **2012**, *1430*, 865–872.
73. Yang, G.D.; Zhan, H.Q.; Chen, W.; Chen, Z.; Yang, Q. Ultrasonic phased array3D Total Focusing Imaging Detection Technology. *Nondestruct. Test.* **2018**, *40*, 64–67. (In Chinese)
74. Liu, W.J.; Qin, H.J.; Wang, J.G.; Wang, S.F. Total focusing 3D imaging-based on ultrasonic phased array. *Transducer Microsyst. Technol.* **2020**, *39*, 26–28+35. (In Chinese)
75. Candès, E.J.; Romberg, J.; Tao, T. Robust uncertainty principles: Exact signal reconstruction from highly incomplete frequency information. *IEEE Trans. Inf. Theory* **2006**, *52*, 489–509. [CrossRef]
76. Candès, E.J. Compressive sampling. *Int. Congr. Math.* **2006**, *3*, 1433–1452.
77. Candes, E.J.; Romberg, J. Quantitative robust uncertainty principles and optimally sparse decompositions. *Found. Comput. Math.* **2006**, *6*, 227–254. [CrossRef]
78. Donoho, D.L. Compressed sensing. *IEEE Trans. Inf. Theory* **2006**, *52*, 1289–1306. [CrossRef]
79. Candes, E.J.; Tao, T. Near-optimal signal recovery from random projections: Universal encoding strategies. *IEEE Trans. Inf. Theory* **2006**, *52*, 5406–5425. [CrossRef]
80. Liu, H.L. *Design and Implementation of Ultrasound Imaging System Based on Compressed Sensing*; University of Chinese Academy of Sciences (National Space Science Center, CAS): Beijing, China, 2017. (In Chinese)
81. Li, M.Q. *Preliminary Research on Ultrasonic Imaging System Based on Compressive Sensing*; University of Chinese Academy of Sciences (National Space Science Center, CAS): Beijing, China, 2016. (In Chinese)
82. Lv, Y.; Wu, W.T.; Li, P. The application of compressed sensing in synthetic transmit aperture medical ultrasound imaging. *Acta Acust.* **2013**, *38*, 426–432. (In Chinese)
83. Zhan, X.L.; Xue, Y. Ultrasonicultrasonic phased array compressed sensing beamforming based on optimal matrix. *J. Civ. Aviat. Univ. China* **2020**, *38*, 31–36. (In Chinese)
84. Azimipanah, A.; Shahbaz Panahi, S. Experimental results of compressive sensing-based imaging in ultrasonic non-destructive testing. In Proceedings of the 2013 5th IEEE International Workshop on Computational Advances in Multi-Sensor Adaptive Processing (CAMSAP), St. Martin, France, 15–18 December 2013; pp. 336–339.
85. Bai, Z.L.; Chen, S.L.; Jia, L.C.; Zeng, Z.M. Compressed Sensing of ultrasonic phased array signal in Turbine Disc Rims Inspection Based on Greedy Algorithms. *J. Mech. Eng.* **2018**, *54*, 33–41. (In Chinese) [CrossRef]
86. Bai, Z.; Chen, S.; Jia, L.; Zeng, Z. Ultrasonic phased array compressive imaging in time and frequency domain: Simulation, experimental verification and real application. *Sensors* **2018**, *18*, 1460. [CrossRef]
87. Bai, Z.L.; Chen, S.L.; Jia, L.C.; Zeng, Z.M. Ultrasonic phased array signal compressed sensing in defect detection. *Acta Acust.* **2019**, *44*, 807–817. (In Chinese)
88. Ouyang, X.Y.; Dai, G.Z.; Li, R.F.; Zeng, Q.G. Ultrasonic phased array industrial imaging research with compressed sensing. In *Applied Mechanics and Materials*; Trans Tech Publications Ltd.: Freienbach, Switzerland, 2013; Volume 347, pp. 317–321.
89. Pyle, R.; Bevan, R.; Wilcox, P. Compression for ultrasonic phased array imaging: Compressive sensing wavelet thresholding. In Proceedings of the Review of Progress in Quantitative Nondestructive Evaluation, Portland, OR, USA, 14–18 July 2019.

90. Wu, B.; Liu, X.B.; Jiao, J.P.; He, C.F. A Full Matrix Data Reconstruction Method of ultrasonic phased array based on Compressed Sensing. *Meas. Control. Technol.* **2021**, *40*, 96–101. (In Chinese)
91. Zheng, Y.; Maev, R.G.; Solodov, I.Y. Review/Sythèse Nonlinear acoustic applications for material characterization: A review. *Can. J. Phys.* **2000**, *77*, 927–967. [CrossRef]
92. Solodov, I.Y. Ultrasonics of non-linear contacts: Propagation, reflection, and NDE-applications. *Ultrasonics* **1998**, *36*, 383–390. [CrossRef]
93. Kawashima, K.; Murase, M.; Yamada, R.; Matsushima, M.; Uematsu, M.; Fujita, F. Nonlinear ultrasonic imaging of imperfectly bonded interfaces. *Ultrasonics* **2006**, *44*, e1329–e1333. [CrossRef] [PubMed]
94. Solodov, I.Y.; Krohn, N.; Busse, G. CAN: An example of nonclassical acoustic nonlinearity in solids. *Ultrasonics* **2002**, *40*, 621–625. [CrossRef]
95. Meziane, A.; Norris, A.N.; Shuvalov, A.L. Nonlinear shear wave interaction at a frictional interface: Energy dissipation and generation of harmonics. *J. Acoust. Soc. Am.* **2011**, *130*, 1820–1828. [CrossRef]
96. Solodov, I. Nonlinear acoustic ndt: Approaches, methods, and applications. In Proceedings of the NDT in Progress, 5th International Workshop of NDT Experts, Prague, Czech Republic, 12–14 October 2009.
97. Aversion, M.A.; Roundhill, D.N.; Powers, J.E. A new imaging technique based on the nonlinear properties of tissues. *Proc. IEEE Ultrason. Symp.* **1997**, *2*, 1561–1566.
98. Averkiou, M.; Powers, J.; Skyba, D.; Bruce, M.; Jensen, S. Ultrasound contrast imaging research. *Ultrasound Q.* **2003**, *19*, 27–37. [CrossRef]
99. Averkiou, M.A. Tissue harmonic imaging. In Proceedings of the 2000 IEEE Ultrasonics Symposium. Proceedings. An International Symposium (Cat. No. 00CH37121), San Juan, PR, USA, 22–25 October 2000; Volume 2, pp. 1563–1572.
100. Qian, Z.W. Nonlinear acoustics in higher-order approximation. *Acta Phys. Sin.* **1995**, *4*, 670.
101. Shen, C.C.; Chou, Y.H.; Li, P.C. Pulse inversion techniques in ultrasonic nonlinear imaging. *J. Med. Ultrasound* **2005**, *13*, 3–17. [CrossRef]
102. Ohara, Y.; Mihara, T.; Sasaki, R.; Ogata, T.; Yamamoto, S.; Kishimoto, Y.; Yamanaka, K. Imaging of closed cracks using nonlinear response of elastic waves at subharmonic frequency. *Appl. Phys. Lett.* **2007**, *90*, 011902. [CrossRef]
103. Sugawara, A.; Jinno, K.; Ohara, Y.; Yamanaka, K. Closed-crack imaging and scattering behavior analysis using confocal subharmonic phased array. *Jpn. J. Appl. Phys.* **2015**, *54*, 07HC08. [CrossRef]
104. Park, C.S.; Kim, J.W.; Cho, S.; Seo, D.C. A high-resolution approach for nonlinear sub-harmonic imaging. *NDT E Int.* **2016**, *79*, 114–122. [CrossRef]
105. Krishnan, S.; Hamilton, J.D.; O'Donnell, M. Suppression of propagating second harmonic in ultrasound contrast imaging. *IEEE Trans. Ultrason. Ferroelectr. Freq. Control* **1998**, *45*, 704–711. [CrossRef]
106. Peng, G.; Faxin, L. Nonlinearultrasonicultrasonic phased array nondestructive testing system and experimental research. *J. Exp. Mech.* **2014**, *29*, 1–11. (In Chinese)
107. Potter, J.N.; Croxford, A.J.; Wilcox, P.D. Nonlinearultrasonicultrasonic phased arrayimaging. *Phys. Rev. Lett.* **2014**, *113*, 144301. [CrossRef]
108. Jiao, J.P.; Yang, S.F.; Ma, T.; He, C.F.; Wu, B. Nonlinear Imaging Usingultrasonicultrasonic phased array under Different Phased Model. *J. Mech. Eng.* **2016**, *52*, 15–24. (In Chinese) [CrossRef]
109. Haupert, S.; Renaud, G.; Schumm, A. Ultrasonic imaging of nonlinear scatterers buried in a medium. *NDT E Int.* **2017**, *87*, 1–6. [CrossRef]
110. Ohara, Y.; Nakajima, H.; Haupert, S.; Tsuji, T.; Mihara, T. Imaging of three-dimensional crack open/closed distribution by nonlinear ultrasonic phased array based on fundamental wave amplitude difference. *Jpn. J. Appl. Phys.* **2020**, *59*, SKKB01. [CrossRef]
111. Xu, Y.Y. *Research on Vibro-Acoustic Modular Detection Technique for Structural Microcrack Based on a Nonlinear Oscillator*; University of Science and Technology of China: Hefei, China, 2015. (In Chinese)
112. Ekimov, A.E.; Didenkulov, I.N.; Kazakov, V.V. Modulation of torsional waves in a rod with a crack. *J. Acoust. Soc. Am.* **1999**, *106*, 1289–1292. [CrossRef]
113. Kazakov, V.V.; Sutin, A.M. Pulsed sounding of cracks with the use of the modulation of ultrasound by vibrations. *Acoust. Phys.* **2001**, *47*, 308–312. [CrossRef]
114. Kim, J.Y.; Yakovlev, V.A.; Rokhlin, S.I. Parametric modulation mechanism of surface acoustic wave on a partially closed crack. *Appl. Phys. Lett.* **2003**, *82*, 3203–3205. [CrossRef]
115. Sutin, A.M.; Donskoy, D.M. Vibro-acoustic modulation nondestructive evaluation technique. In Proceedings of the Nondestructive Evaluation of Aging Aircraft, Airports, and Aerospace Hardware II. International Society for Optics and Photonics, San Antonio, TX, USA, 31 March–2 April 1998; Volume 3397, pp. 226–237.
116. Sutin, A.M.; Johnson, P.A. Nonlinear elastic wave NDE II. Nonlinear wave modulation spectroscopy and nonlinear time-reversed acoustics. *AIP Conf. Proc.* **2005**, *760*, 385–392.
117. Duffour, P.; Morbidini, M.; Cawley, P. A study of the vibroacoustic modulation technique for the detection of cracks in metals. *J. Acoust. Soc. Am.* **2006**, *119*, 1463–1475. [CrossRef]
118. Ohara, Y.; Yamamoto, S.; Mihara, T.; Yamanaka, K. Ultrasonic evaluation of closed cracks using subharmonic phased array. *Jpn. J. Appl. Phys.* **2008**, *47*, 3908. [CrossRef]

119. Ohara, Y.; Mihara, T.; Yamanaka, K. Effect of adhesion force between crack planes on subharmonic and DC responses in nonlinear ultrasound. *Ultrasonics* **2006**, *44*, 194–199. [CrossRef]
120. Yamanaka, K.; Ohara, Y. Selectivity enhancement of subharmonicultrasonic phased arrayfor crack evaluation (SPACE). *AIP Conf. Proc.* **2009**, *1096*, 824–831.
121. Ohara, Y.; Horinouchi, S.; Hashimoto, M.; Shintaku, Y.; Yamanaka, K. Nonlinear ultrasonic imaging method for closed cracks using subtraction of responses at different external loads. *Ultrasonics* **2011**, *51*, 661–666. [CrossRef]
122. Ohara, Y.; Takahashi, K.; Murai, S.; Yamanaka, K. High-selectivity imaging of closed cracks using elastic waves with thermal stress induced by global preheating and local cooling. *Appl. Phys. Lett.* **2013**, *103*, 031917. [CrossRef]
123. Mihara, T.; Konishi, G.; Miura, Y.; Ishida, H. Accurate sizing of closed crack using nonlinear ultrasound of SPACE with high voltage transformer pulser technique. In *AIP Conference Proceedings*; American Institute of Physics: College Park, MD, USA, 2014; Volume 1581, pp. 727–732.
124. Ling, T.H.; Zheng, H.; He, H.R.; Hu, L.C.; Cao, Y.G. Research on Micro-crack Localization Imaging Based on Vibro-Acoustic Modulation. *Acta Metrol. Sin.* **2020**, *41*, 214–220. (In Chinese)
125. Jiao, J.P.; He, C.F.; Wu, B.; Drinkwater, S.A.; Neild, P.D. Wilcox. Vibro-modulation and guided wave techniques for contact defect detection in plate. *Acta Acust.* **2009**, *34*, 242–248. (In Chinese)